

國立臺灣大學理學院物理學系

碩士論文

Department of Physics

College of Science

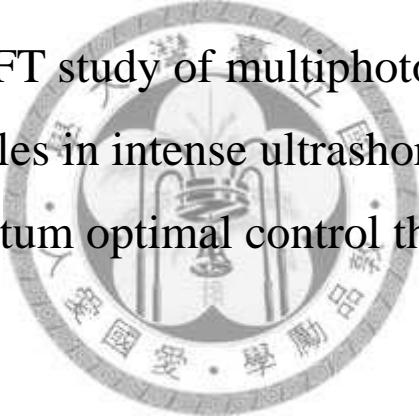
National Taiwan University

Master Thesis

以第一原理含時密度泛函理論研究雙原子分子在超短

強場雷射下的多光子效應及量子最佳控制理論

*Ab initio* TDDFT study of multiphoton dynamics of  
diatomic molecules in intense ultrashort laser fields and  
quantum optimal control theory



陳佑航

Chen, Yu-Hang

指導教授：朱時宜 博士

Advisor: Chu, Shih-I, Ph.D.

中華民國 98 年 8 月

August, 2009

## 中文摘要

我們以第一原理計算和研究雙原子分子在超短強場雷射下的多光子過程，並且使用了對遠距位能修正過的含時密度泛函理論 (time-dependent density functional theory) 來處理多電子分子系統。為了得到準確並有效率的結果，我們採用推廣到雙元子系統的廣義擬似譜法 (generalized pseudospectral method) 來做數值處理。在多光子電離的計算中，可發現分子軌域的排列方向會直接的影響不同軌域的電離順序。而我們也獲得詳細的高次諧波頻譜 (high harmonic generation) 及比較了最高電子佔有軌域做出的貢獻。我們還發現到一氧化碳分子帶有的永久電偶極矩破壞了反轉對稱，從而產生原子系統不會出現的偶數高次諧波。

另外在本篇論文中，我們用最佳控制理論 (optimal control theory) 成功的控制且達到在雙能階系統下的時變目標，並應用共軛梯度法 (conjugate gradient algorithm) 大幅減少數值迭代所需的次數。



## Abstract

We present an *ab initio* study of the time-dependent density-functional theory (TDDFT) with proper asymptotic long-range potential for nonperturbative treatment of multi-photon processes of diatomic molecules in strong laser field. For accurate and efficient treatment of the TDDFT equations, the generalized pseudospectral method (GPS) is extended to two-center molecules system. The procedure allows nonuniform and optimal spatial grid discretization of the Hamiltonian in prolate spheroidal coordinates and the time propagation using the split-operator technique in the energy representation.

The multiphoton ionization and high-order harmonic generation (HHG) of diatomic molecules  $N_2$ ,  $CO$ , and  $O_2$  in intense short laser pulse fields are calculated in detail. We observe both the electronic binding energy and the orientation of the orbitals affect the ionization rate. In the analysis of HHG, the highest occupied molecular orbital (HOMO) has dominant contribution, but accurate results have to be obtained with all-electron study. The  $CO$  molecule has a small permanent dipole moment cause the different nonlinear optical response to homonuclear molecules such as generating both even and odd harmonics.

We also practice the optimal control theory using time-dependent targets on the two-level system with use of the conjugate gradient algorithm, therefore greatly reducing the number of iterations to reach convergence.

# Contents

Chapter 1 Introduction.....	1
Chapter 2 Theory of electron structure in diatomic molecules .....	3
2.1 Ground state density functional theory.....	3
2.1.1 Hohenberg-Kohn theorems.....	3
2.1.2 Kohn-Sham equations .....	6
2.1.3 Approximations for the exchange-correlation functional.....	7
2.2 Time-dependent density functional theory .....	8
2.3 Generalized pseudospectral method for two-center systems.....	10
2.4 Numerical solutions of the TDDFT equation .....	13
Chapter 3 Optimal control theory.....	17
3.1 Basic theory .....	17
3.2 Final-time targets and algorithms .....	19
3.3 Time-dependent targets and algorithms.....	22
3.4 Conjugate gradient method.....	23
3.5 Constraints on the optimal fields .....	24
Chapter 4 Results and discussion .....	26
4.1 Orbital energies.....	26
4.2 Multiphoton ionization .....	28
4.3 High-order harmonic generation .....	32
4.4 OCT on two-level system .....	42
Chapter 5 Conclusion and perspectives.....	47
Bibliography .....	48

# List of Figures

Figure 4-1 The time-dependent population of electrons of individual spin orbitals of O <sub>2</sub> in 20-optical-cycle, 800 nm, sin <sup>2</sup> laser pulses. The laser intensities is 10 <sup>14</sup> W/cm <sup>2</sup> .....	28
Figure 4-2 The time-dependent population of electrons of individual spin orbitals of N <sub>2</sub> in 20-optical-cycle, 800 nm, sin <sup>2</sup> laser pulses. The laser intensities are (a) 5 × 10 <sup>13</sup> , (b) 10 <sup>14</sup> W/cm <sup>2</sup> .....	29
Figure 4-3 The time-dependent population of electrons of individual spin orbitals of CO in 20-optical-cycle, 800 nm, sin <sup>2</sup> laser pulses. The laser intensities are (a) 5 × 10 <sup>13</sup> , (b) 10 <sup>14</sup> W/cm <sup>2</sup> .....	30
Figure 4-4 The HHG power spectrum of N <sub>2</sub> in the field intensity (a) 5 × 10 <sup>13</sup> W/cm <sup>2</sup> and (b) 10 <sup>14</sup> W/cm <sup>2</sup> , of CO in the field intensity (c) 5 × 10 <sup>13</sup> W/cm <sup>2</sup> and (d) 10 <sup>14</sup> W/cm <sup>2</sup> , and of O <sub>2</sub> in the field intensity (e) 5 × 10 <sup>13</sup> W/cm <sup>2</sup> and (f) 10 <sup>14</sup> W/cm <sup>2</sup> , 800nm, sin <sup>2</sup> laser pulses.....	33
Figure 4-5 Comparison of the induced dipole moment of N <sub>2</sub> from different spin orbital in 10 <sup>14</sup> W/cm <sup>2</sup> , 800nm, sin <sup>2</sup> laser pulses .....	34
Figure 4-6 (a) Comparison of the total HHG power spectrum and the partial contributions from HOMO of N <sub>2</sub> , and (b) from different spin orbital in 10 <sup>14</sup> W/cm <sup>2</sup> , 800nm, sin <sup>2</sup> laser pulses .....	35
Figure 4-7 Comparison of the induced dipole moment of CO from different spin orbital in 10 <sup>14</sup> W/cm <sup>2</sup> , 800nm, sin <sup>2</sup> laser pulses.....	36
Figure 4-8 (a) Comparison of the total HHG power spectrum and the partial contributions from HOMO of CO, and (b) from different spin orbital in	

10 <sup>14</sup> W/cm <sup>2</sup> , 800nm, sin <sup>2</sup> laser pulses .....	37
Figure 4-9 Comparison of the induced dipole moment of O <sub>2</sub> from different spin orbital in 10 <sup>14</sup> W/cm <sup>2</sup> , 800nm, sin <sup>2</sup> laser pulses.....	38
Figure 4-10 (a) Comparison of the total HHG power spectrum and the partial contributions from HOMO of O <sub>2</sub> , and (b) from different spin orbital in 10 <sup>14</sup> W/cm <sup>2</sup> , 800nm, sin <sup>2</sup> laser pulses .....	39
Figure 4-11 Time profiles for (a) N <sub>2</sub> and (b) CO. Laser intensity used is 10 <sup>14</sup> W/cm <sup>2</sup> , wavelength used is 800nm, with 20-optical-cycle in pulse duration.....	41
Figure 4-12 Optimization of the $ a\rangle \rightarrow  b\rangle$ transition. (a) Optimized field. (b) Time evolution of the occupation numbers for the system propagated with the optimized pulse. (c) Convergence of J <sub>1</sub> and J <sub>2</sub> over the iterations. ....	43
Figure 4-13(a) Optimized field. (b) Targets and time evolution of the occupation numbers. (c) Convergence of J <sub>1</sub> and J <sub>2</sub> over the iterations ...	45
Figure 4-14(a) Optimized field. (b) Targets and time evolution of the occupation numbers. (c) Convergence of J <sub>1</sub> and J <sub>2</sub> over the iterations ...	46

# List of tables

Table I (A) Spin orbital energies of diatomic molecules of present DFT calculations with $LB_{\alpha}$ potential(a.u.). (B) Experimental vertical ionization potentials(a.u.). .....	26
Table II HOMO energies of $N_2$ and CO molecules in DC electric field(positive field direction is from C to O).....	27



# Chapter 1

## Introduction

Current laser technology has opened up a new field of study, the nonlinear nonperturbative response of matter to intense ultrashort laser pulses [1]. This led to the discovery of many new nonlinear nonperturbative optical phenomena and processes such as above threshold ionization, multiphoton ionization (MPI), and high-order harmonic generation (HHG) which is one of the most rapidly developing topics in strong field physics in the past decade. Examples of the potential applications of the HHG include following: the development of coherent soft x-ray laser light source and nonlinear optics in the extreme ultraviolet regime [2], attosecond laser pulses [3], and comb laser technology [4, 5]. Recently, both experimental and theoretical investigations have focus on the diatomic molecules in intense laser fields [6]. Comparing to the atoms, the extra internuclear degree of freedom make the phenomena within considerably more complicated and various.

Approximate models, such as ADK [7] and KFR(or Keldysh-Faisal-Reiss) [8, 9] which are based on single active electron [10] and other approximation, consider only the HOMO contributing to the molecular ionization. However, these models sometimes make failure prediction such as the ionization suppression of  $F_2$  [11, 12]. Thus, it is necessary to describe such strong-field processes using *ab initio* wave-function approach. Then we have to solve the time-dependent Schrodinger equation of many-electron systems in space and time, which is beyond the capability of current computer technology. To overcome this, time-dependent density functional



theory with self-interaction correction has been recently developed for nonperturbative treatment of many-electron atomic systems in strong fields [13-15].

The technology for ultrafast laser pulses shaping is rapidly and currently being developed and the introduction of closed-loop learning control techniques [16] in the laboratory has advanced the realization of many control experiments. These experiments include manipulating electronic excitation [17], compressing optical pulse [18], enhancement of HHG [19], and redirecting energy transfer in bio-molecules [20].

Optimal control theory (OCT) is a field of mathematics dates back to the late 1950s and widely applied in engineering. The application of OCT to quantum mechanics started in the 1980s [21, 22]. Calculated pulse shapes may not only be used to directly employ in the experimental setup, e.g., as an initial guess for genetic algorithms, but also let us explore the insight of physics inside the control system.

This thesis is organized as follows. We introduce the basic theorems of ground state density functional theory and time-dependent density functional theory in the first two sections of chapter 2. Then, we outline the generalized pseudospectral method for nonuniform and optimal spatial discretization of the two-center system. In chapter 3, we review the concept and algorithm of optimal control theory. In chapter 4, we investigate multiphoton ionization and high-order harmonic generation of homo-nuclear and hetero-nuclear diatomic molecules such as  $N_2$ ,  $CO$ , and  $O_2$ , respectively. And next we show the results of quantum control. Lastly, chapter 5 contains concluding remarks and possible future extension of the current work.

# Chapter 2

## Theory of electron structure in diatomic molecules

### 2.1 Ground state density functional theory

#### 2.1.1 Hohenberg-Kohn theorems

The central statement of formal density functional theory is the Hohenberg-Kohn theorem [23] which, for non-degenerate ground states, can be summarized in the following three statements:

1. The ground state electron density  $\rho(\mathbf{r})$  uniquely determines the ground-state wave function  $\Psi[\rho]$  as well as the external potential  $v = v[\rho]$ . As a consequence, any observable of a static many-particle system is a functional of its ground-state density.

Here is the proof: Consider a system of  $N$  electrons described by the Hamiltonian

$$\begin{aligned}\hat{H}_V &= \hat{T} + \hat{V} + \hat{V}_{ee} \\ &= -\sum_{i=1}^N \frac{\nabla_i^2}{2} + \sum_{i=1}^N v(\mathbf{r}_i) + \frac{1}{2} \sum_{i=1}^N \sum_{\substack{j=1 \\ i \neq j}}^N \frac{1}{|\mathbf{r}_i - \mathbf{r}_j|},\end{aligned}\quad (2.1)$$

with the kinetic, potential and interaction energy operators  $\hat{T}$ ,  $\hat{V}$ , and  $\hat{V}_{ee}$  (atomic units are used throughout.)

For simplicity, assume the external potential  $v(\mathbf{r})$  leads to a non-degenerate ground state  $\Psi$ :

$$\hat{H}_v \Psi = E_g \Psi, \quad (2.2)$$

for each  $\Psi$  we then have the ground-state density

$$\rho(\mathbf{r}) = \langle \Psi | \hat{n}(\mathbf{r}) | \Psi \rangle. \quad (2.3)$$

We want to show that two different ground states  $\Psi(\mathbf{r}) \neq \Psi'(\mathbf{r})$  (arising from two different potentials  $v(\mathbf{r}) \neq v'(\mathbf{r}) + \text{const}$ ) always lead to different ground-state densities  $\rho(\mathbf{r}) \neq \rho'(\mathbf{r})$ .

$$E_g = \langle \Psi | \hat{H}_v | \Psi \rangle < \langle \Psi' | \hat{H}_v | \Psi' \rangle = \langle \Psi' | \hat{H}_{v'} + \hat{V} - \hat{V}' | \Psi' \rangle = E'_g + \int d^3\mathbf{r} \rho'(\mathbf{r})(v(\mathbf{r}) - v'(\mathbf{r})). \quad (2.4)$$

Due to the restriction to non-degenerate ground state, equation (2.4) is a strict inequality.

An analogous argument starting with  $E'_g$  leads to

$$E'_g < E_g + \int d^3\mathbf{r} \rho(\mathbf{r})(v(\mathbf{r}) - v'(\mathbf{r})). \quad (2.5)$$

Assuming  $\rho(\mathbf{r}) = \rho'(\mathbf{r})$ , the addition of equation (2.4) and equation (2.5) leads to the contradiction

$$E'_g + E_g < E_g + E'_g. \quad (2.6)$$

Thus we derived that two different potentials could not lead to the same charge density.

2. The ground-state energy  $E_0$  and the ground-state density  $\rho_0(\mathbf{r})$  of a system characterized by the potential  $v_0(\mathbf{r})$  can be obtained from a variational principle which involves only the density, then the ground state energy can be written as a functional of the density,  $E_{v_0}[\rho]$ , which gives the ground-state energy  $E_0$  if and only if the true ground-state density  $\rho_0(\mathbf{r})$  is inserted. For all other densities  $\rho(\mathbf{r})$ , the inequality

$$E_0 = E_{v_0}[\rho_0] < E_{v_0}[\rho], \quad (2.7)$$

holds.

From the Hohenberg-Kohn variational principle, i.e., the second statement given above, the ground-state density  $\rho(\mathbf{r})$  corresponding to the external potential  $v(\mathbf{r})$  can be obtained as solution of the Euler equation

$$\frac{\delta}{\delta\rho(\mathbf{r})} \left[ E_{v_0}[\rho] - \mu \int d^3\mathbf{r}' \rho'(\mathbf{r}') \right] = 0. \quad (2.8)$$

3. There exists a functional  $F[\rho]$  such that the energy functional can be written as

$$E_{v_0}[\rho] = F[\rho] + \int d^3\mathbf{r} \rho(\mathbf{r})v_0(\mathbf{r}), \quad (2.9)$$

the functional  $F[\rho]$  is universal in the sense that, for a given particle-particle interaction (the Coulomb interaction in our case), it is independent of the potential  $v_0(\mathbf{r})$  of the particular system under consideration, i.e., it has the same functional form for all systems.

The formal definition of the Hohenberg-Kohn functional  $F[\rho]$  is well known,

$$F[\rho] = \langle \Psi[\rho] | \hat{T} + \hat{V}_{ee} | \Psi[\rho] \rangle = T[\rho] + J[\rho], \quad (2.10)$$

where  $\Psi[\rho]$  is that N-electron wave-function which yields the density  $\rho$  and minimizes the expectation value of  $\hat{T} + \hat{V}_{ee}$ . However, the explicit density dependence of  $F[\rho]$  remains unknown. Approximations have been suggested, the oldest one being the well-known Thomas-Fermi approximation (which precedes the Hohenberg-Kohn theorem historically).

Most practical applications of DFT make use of an extension of the original theory which uses the partial densities of electrons with different spin  $\sigma$  as independent variables,

$$n_{i\sigma}(\mathbf{r}) = \sum |\Psi_{i\sigma}(\mathbf{r})|^2, \quad (2.11)$$

rather than using the total density.

## 2.1.2 Kohn-Sham equations

Density-functional theory can be implemented in many ways. The minimization of an explicit energy functional, is not normally the most efficient among them. Much more widely used is the Kohn-Sham approach [24]. Interestingly, this approach owes its success and popularity partly to the fact that it does not exclusively work in terms of the density, but brings a special kind of wave functions (single-particle orbitals) back into the game. As a consequence DFT then looks formally like a single-particle theory, although many-body effects are still included.

In the KS formulation, the Hamiltonian for N-electron system:

$$\hat{H}_{KS}(\mathbf{r})\Psi_{i\sigma}(\mathbf{r}) = \left[ -\frac{\nabla^2}{2} + v_{eff,\sigma}(\mathbf{r}) \right] \Psi_{i\sigma}(\mathbf{r}) = \epsilon_{i\sigma} \Psi_{i\sigma}(\mathbf{r}), \quad (2.12)$$

$i = 1, 2, \dots, N_\sigma$

where  $v_{eff}(\mathbf{r})$  is the effective KS potential. The total density is given by

$$\rho(\mathbf{r}) = \sum_{i=1}^N |\Psi_{i\sigma}(\mathbf{r})|^2 = \rho_\uparrow(\mathbf{r}) + \rho_\downarrow(\mathbf{r}), \quad (2.13)$$

and the ground-state wave function is determined by

$$\Psi = \frac{1}{\sqrt{N!}} \det[\Psi_1 \Psi_2 \dots \Psi_N]. \quad (2.14)$$

The total energy of the ground state is obtained by the minimization of the Hohenberg-Kohn energy functional

$$E[\rho_\uparrow, \rho_\downarrow] = T_s[\rho] + J[\rho] + E_{xc}[\rho_\uparrow, \rho_\downarrow] + \int v_{ext}(\mathbf{r})\rho(\mathbf{r})d\mathbf{r}, \quad (2.15)$$

here  $T_s$  is the noninteracting KS kinetic energy,

$$T_s = \sum_i^N \langle \Psi_{i\sigma} | -\frac{\nabla^2}{2} | \Psi_{i\sigma} \rangle, \quad (2.16)$$

$v_{\text{ext}}(\mathbf{r})$  is the external potential due to the electron-nucleus interaction,  $J[\rho]$  is the classical electron-electron repulsive energy,

$$J[\rho] = \frac{1}{2} \iint \frac{\rho(\mathbf{r})\rho(\mathbf{r}')}{|\mathbf{r}-\mathbf{r}'|} d\mathbf{r}d\mathbf{r}', \quad (2.17)$$

and  $E_{\text{xc}}[\rho]$  is the exchange-correlation energy functional. Minimization of the total energy functional, equation (2.13) subject to the constraint

$$\int \rho_\sigma(\mathbf{r}) d\mathbf{r} = N_\sigma. \quad (2.18)$$

Give rise to the KS equations with the effective potential

$$\begin{aligned} v_{\text{ext},\sigma}(\mathbf{r}) &= v_{\text{ext}}(\mathbf{r}) + \frac{\delta J[\rho]}{\delta \rho_\sigma(\mathbf{r})} + \frac{\delta E_{\text{xc}}[\rho_\uparrow, \rho_\downarrow]}{\delta \rho_\sigma(\mathbf{r})}, \\ &= v_{\text{ext}}(\mathbf{r}) + \int \frac{\rho(\mathbf{r}')}{|\mathbf{r}-\mathbf{r}'|} d\mathbf{r}' + v_{\text{xc},\sigma}(\mathbf{r}) \end{aligned}, \quad (2.19)$$

where  $v_{\text{xc}}(\mathbf{r})$  is the exchange-correlation potential,

$$v_{\text{xc},\sigma}(\mathbf{r}) = \frac{\delta E_{\text{xc}}[\rho_\uparrow, \rho_\downarrow]}{\delta \rho_\sigma(\mathbf{r})}. \quad (2.20)$$

The KS equations are to be solved self-consistently, starting from some initial estimate of the density  $\rho_\sigma(\mathbf{r})$ , until convergence is reached.

### 2.1.3 Approximations for the exchange-correlation functional

While DFT itself does not give any hint on how to construct approximate exchange-correlation functionals, local density approximation (LDA) has remained the approximation of choice for quite many years after the formulation of the Kohn-Sham theorem. In LDA, the exchange-correlation energy is given by

$$E_{\text{xc}}^{\text{LDA}}[\rho] = \int d^3\mathbf{r} \rho(\mathbf{r}) e_{\text{xc}}^{\text{unif}}[\rho(\mathbf{r})], \quad (2.21)$$

where  $e_{xc}^{unif}$  is the exchange-correlation energy per particle of an electron gas with spatially uniform density  $\rho$ . It can be obtained from quantum Monte Carlo calculations and simple parameterizations are available. By its very construction, the LDA is expected to be a good approximation for spatially slowly varying densities. Although this condition is hardly ever met for real electronic systems, LDA has proved to be remarkably accurate for a wide variety of systems. In the quest for improved functionals, an important breakthrough was achieved with the emergence of the so-called generalized gradient approximations (GGA) [25]. Within GGA, the exchange-correlation energy for spin-unpolarized systems is written as

$$E_{xc}^{GGA}[\rho] = \int d^3\mathbf{r} f(\rho(\mathbf{r}), \nabla\rho(\mathbf{r})). \quad (2.22)$$

While the input in LDA is unique, the function  $f$  in GGA is not and many different forms have been suggested. When constructing a GGA one usually tries to incorporate a number of known properties of the exact functional into the restricted functional form of the approximation. The impact of GGAs has been quite dramatic, especially in quantum chemistry where DFT is now competitive in accuracy with more traditional methods while being computationally less expensive.

## 2.2 Time-dependent density functional theory

The central theorem of time-dependent density functional theory (TDDFT) is from the concept of ground state density functional theory. It proves there is a one-to-one correspondence between the time-dependent external potential and the electronic density. With this theory, we could develop a Kohn-Sham like scheme to solve time-dependent Schrödinger equation. Although the one-to-one correspondence has

given us in principle an exact description of many-electron quantum mechanics in a time-dependent potential, the scheme is still incomplete without some approximation to the missing exchange-correlation potential. Then the adiabatic approximation [13, 26] is often used, which we ignore all dependence on the past, and allow only a dependence on the instantaneous density,

$$V_{xc}^{adia}[\rho](\mathbf{r}, t) = V_{xc}[\rho](\mathbf{r})|_{\rho(\mathbf{r}')=\rho(\mathbf{r}', t)}. \quad (2.23)$$

We begin by a set of time-dependent one-electron Schrödinger-like Kohn-Sham equations for N-electron atomic or molecular systems,

$$i \frac{\partial}{\partial t} \psi_{i\sigma}(\mathbf{r}, t) = H(\mathbf{r}, t) \psi_{i\sigma}(\mathbf{r}, t) = \left[ -\frac{1}{2} \nabla^2 + v_{eff,\sigma}(\mathbf{r}, t) \right] \psi_{i\sigma}(\mathbf{r}, t) \quad (2.24)$$

,  $i=1, 2, \dots, N_\sigma$ ,

where  $N_\sigma (= N_\uparrow \text{ or } N_\downarrow)$  is the total number of electrons for a given spin  $\sigma$ .

The total number of electrons in the system is  $N = \sum_\sigma N_\sigma$ . The time-dependent effective potential  $v_{eff,\sigma}(\mathbf{r}, t)$  is a functional of the electron spin-densities  $\rho_\sigma(\mathbf{r}, t)$ . The total electron density at time  $t$  is determined by the set of occupied single-electron Kohn-Sham spin-orbital wave functions  $\psi_{i\sigma}$  as

$$\rho(\vec{r}, t) = \sum_\sigma \sum_{i=1}^{N_\sigma} \psi_{i\sigma}^* \psi_{i\sigma} = \sum_\sigma \sum_{i=1}^{N_\sigma} \rho_{i\sigma}(\mathbf{r}, t) = \rho_\uparrow(\mathbf{r}, t) + \rho_\downarrow(\mathbf{r}, t). \quad (2.25)$$

The effective potential  $v_{eff,\sigma}(\rho; \vec{r}, t)$  in equation (2.24) can be written in the general form

$$v_{eff,\sigma}(\rho; \mathbf{r}, t) = v_H(\mathbf{r}, t) + v_{ext}(\mathbf{r}, t) + v_{xc,\sigma}(\mathbf{r}, t), \quad (2.26)$$

where

$$v_H(\mathbf{r}, t) = \int \frac{\rho(\mathbf{r}', t)}{|\mathbf{r} - \mathbf{r}'|} d\mathbf{r}', \quad (2.27)$$

is the Hartree potential due to electron-electron Coulomb interaction,  $v_{ext}(\vec{r}, t)$  is the external potential due to the interaction of the electron with the external laser field and



the nuclei.  $v_{xc,\sigma}(\mathbf{r},t)$  is the time-dependent exchange-correlation potential.

Note that if the conventional explicit exchange-correlation energy functional forms taken from local spin density approximation or generalized gradient approximation are used, the corresponding exchange-correlation potential  $v_{xc,\sigma}(\mathbf{r},t)$  will not possess the correct long-range asymptotic  $(-1/r)$  behavior. Here, we adopt the improved LB potential[27],  $v_{xc,\sigma}^{LB\alpha}$ , which contains two empirical parameters  $\alpha$  and  $\beta$  and has the following form

$$v_{xc,\sigma}^{LB\alpha}(\mathbf{r},t) = \alpha v_{x,\sigma}^{LSDA}(\mathbf{r},t) + v_{c,\sigma}^{LSDA}(\mathbf{r},t) - \frac{\beta x_\sigma^2(\mathbf{r},t) \rho_\sigma^{1/3}(\mathbf{r},t)}{1 + 3\beta x_\sigma(\mathbf{r},t) \ln\{x_\sigma(\mathbf{r},t) + [x_\sigma^2(\mathbf{r},t) + 1]^{1/2}\}}, \quad (2.28)$$

here,  $\rho_\sigma$  is the electron density with spin  $\sigma$ , and we use  $\alpha = 1.19$  and  $\beta = 0.01$ . The first two terms in equation (2.28),  $v_{x,\sigma}^{LSDA}(\mathbf{r},t)$  and  $v_{c,\sigma}^{LSDA}(\mathbf{r},t)$  are the LSDA exchange and correlation potentials that do not have the correct asymptotic behavior. The last term is the nonlocal gradient correction with  $x_\sigma(\mathbf{r}) = |\nabla\rho_\sigma(\mathbf{r})|/\rho_\sigma^{4/3}(\mathbf{r})$ , which ensures the proper long-range asymptotic potential  $v_{xc,\sigma}^{LB\alpha}(\bar{r},t) \rightarrow -1/r$  as  $r \rightarrow \infty$ . For the time-independent case, this exchange-correlation LB $\alpha$  potential has been found to be reliable for atomic and molecular DFT calculations.

## 2.3 Generalized pseudospectral method for two-center systems

In this section, we present the procedure of the generalized pseudospectral (GPS) method for non-uniform and optimal spatial discretization of diatomic systems[28-30]. We shall use the prolate spheroidal coordinates for the description of the system. Prolate

spheroidal coordinates  $(\xi, \eta, \psi)$  are a three-dimensional system of coordinates obtained by rotating a two-dimensional elliptic coordinate system about the focal axis of the ellipse. The angle of rotation is defined by  $\phi (0 \leq \phi \leq 2\pi)$ . With the foci located at  $\pm a$  along the  $z$ -axis and  $r_1$  and  $r_2$  denoting the distances to the two foci, the dimensionless coordinates  $(\xi, \eta)$  are defined as [31]

$$\begin{aligned}\xi &= \frac{r_1 + r_2}{2a} \quad (1 \leq \xi \leq \infty), \\ \eta &= \frac{r_1 - r_2}{2a} \quad (-1 \leq \eta \leq 1),\end{aligned}\tag{2.29}$$

and the back transformation to Cartesian coordinates is

$$\begin{aligned}x &= a\sqrt{(\xi^2 - 1)(1 - \eta^2)} \cos \phi \\ y &= a\sqrt{(\xi^2 - 1)(1 - \eta^2)} \sin \phi \\ z &= a\xi\eta\end{aligned}\tag{2.30}$$

The Laplacian in these coordinates is

$$\begin{aligned}\nabla^2 &= \frac{1}{a^2} \frac{1}{(\xi^2 - \eta^2)} \left( \frac{\partial}{\partial \xi} (\xi^2 - 1) \frac{\partial}{\partial \xi} + \frac{\partial}{\partial \eta} (1 - \eta^2) \frac{\partial}{\partial \eta} \right. \\ &\quad \left. + \frac{\xi^2 - \eta^2}{(\xi^2 - 1)(1 - \eta^2)} \frac{\partial}{\partial \phi^2} \right),\end{aligned}\tag{2.31}$$

and the volume element is

$$dV = a^3 (\xi^2 - \eta^2) d\xi d\eta d\phi.\tag{2.32}$$

Due to the axial symmetry with respect to the  $z$ -axis, the projection  $m$  of the angular momentum onto the molecular axis is conserved. Thus the wave function  $\Psi(\xi, \eta, \phi)$  can be represented in a separable form,

$$\Psi(\xi, \eta, \phi) = \varphi(\xi, \eta) e^{im\phi} \quad (m = 0, \pm 1, \pm 2, \dots).\tag{2.33}$$

The unperturbed Hamiltonian for diatomic molecules is

$$\hat{H}_0(\mathbf{r}) = -\frac{\nabla^2}{2} - \frac{Z_1}{|\mathbf{R}_1 - \mathbf{r}|} - \frac{Z_2}{|\mathbf{R}_2 - \mathbf{r}|} + v_{ee}(\mathbf{r}) + v_{xc,\sigma}(\mathbf{r}), \quad (2.34)$$

$Z_1$  and  $Z_2$  are the electric charges of the two nuclei.  $\mathbf{R}_1$  and  $\mathbf{R}_2$  are the position of them which have been put on the foci along  $z$ -axis. Direct applying this Hamiltonian into the pseudospectral discretization leads to an asymmetric eigenvalue problem. We will use the alternative but equivalent variational form of the Schrödinger equation

$$\frac{\delta \int d^3\mathbf{r} \Psi^* (\hat{H} - E) \Psi}{\delta \Psi^*} = 0. \quad (2.35)$$

Also for even and odd  $m$ , we should use different expressions for kinetic energy operator. This is done to ensure accurate numerical solutions of the differential equations for both even and odd projections of angular momentum (note that the exact eigenfunctions have factors  $(\xi^2 - 1)^{|m|/2} (1 - \eta^2)^{|m|/2}$  which are non-analytical at nuclei for odd  $|m|$ ). Now we discretize equation (2.34) with GPS method and have the following equation for even  $m$  values,

$$\sum_{i'j'} \left[ T_{ij;i'j'}^e + \left( \frac{m^2}{2a^2(\xi_i^2 - 1)(1 - \eta_j^2)} - \frac{Z_1(\xi_i - \eta_j)}{a(\xi_i^2 - \eta_j^2)} - \frac{Z_2(\xi_i - \eta_j)}{a(\xi_i^2 - \eta_j^2)} + v_{ee}(\xi_i, \eta_j) + v_{xc,\sigma}(\xi_i, \eta_j) \right) \delta_{ii'} \delta_{jj'} \right] \Phi_{m;i'j'} = E \Phi_{m;ij} \quad (2.36)$$

and odd  $m$  values,

$$\sum_{i'j'} \left[ T_{ij;i'j'}^o + \left( \frac{m^2 - 1}{2a^2(\xi_i^2 - 1)(1 - \eta_j^2)} + \frac{1 + \xi_i^2}{a^2(\xi_i^2 - \eta_j^2)} - \frac{Z_1(\xi_i - \eta_j)}{a(\xi_i^2 - \eta_j^2)} - \frac{Z_2(\xi_i - \eta_j)}{a(\xi_i^2 - \eta_j^2)} + v_{ee}(\xi_i, \eta_j) + v_{xc,\sigma}(\xi_i, \eta_j) \right) \delta_{ii'} \delta_{jj'} \right] \Phi_{m;i'j'} = E \Phi_{m;ij} \quad (2.37)$$

Here the quantities  $\Phi_{m;ij}$  are related to the wave function at the discretized coordinates,

$$\Psi_m(\xi_i, \eta_j) = \frac{\Phi_{m;ij}}{\sqrt{\xi_i'} \eta_j'} \sqrt{\frac{1-y_j^2}{1+x_i}} \frac{P_{N_x}(x_i) P_{N_y}'(y_j)}{\sqrt{(\xi_i^2 - \eta_j^2)}}, \quad (2.38)$$

$P_{N_x}(x)$  and  $P'_{N_y}(y)$  are the Legendre polynomial and it's derivative. The kinetic energy matrices  $T_{ij;i'j'}^e$  and  $T_{ij;i'j'}^o$  are calculated as follow [32],

$$\begin{aligned} T_{ij;i'j'}^o &= \frac{1}{2a^2} \frac{1}{\sqrt{\xi_i'} \eta_j'} \frac{1}{\sqrt{(\xi_i^2 - \eta_j^2)}} \frac{1}{\sqrt{\xi_i'} \eta_j'} \frac{1}{\sqrt{(\xi_i^2 - \eta_j^2)}} \\ &\times \left( \delta_{jj'} \sqrt{1+x_i} \sqrt{1+x_i'} \sum_{k=1}^{N_x} \frac{\xi_i^2 - 1}{\xi_k' (1+x_k)} d_{ki}^x d_{ki'}^x \right. \\ &\left. + \delta_{ii'} \sqrt{1-y_j^2} \sqrt{1-y_j'^2} \sum_{k=1}^{N_y} \frac{1-\eta_k^2}{\eta_k' (1-y_k^2)} d_{kj}^y d_{kj'}^y \right), \end{aligned} \quad (2.39)$$

and

$$\begin{aligned} T_{ij;i'j'}^e &= \frac{1}{2a^2} \frac{1}{\sqrt{\xi_i'} \eta_j'} \frac{1}{\sqrt{(\xi_i^2 - \eta_j^2)}} \frac{1}{\sqrt{\xi_i'} \eta_j'} \frac{1}{\sqrt{(\xi_i^2 - \eta_j^2)}} \\ &\times \left( \delta_{jj'} \sqrt{\frac{1+x_i}{\xi_i^2 - 1}} \sqrt{\frac{1+x_i'}{\xi_i'^2 - 1}} \xi_i \xi_i' \sum_{k=1}^{N_x} \frac{(\xi_i^2 - 1)^2}{\xi_k' (1+x_k)} d_{ki}^x d_{ki'}^x \right. \\ &\left. + \delta_{ii'} \sqrt{\frac{1-y_j^2}{1-\eta_j^2}} \sqrt{\frac{1-y_j'^2}{1-\eta_j'^2}} \sum_{k=1}^{N_y} \frac{(1-\eta_k^2)^2}{\eta_k' (1-y_k^2)} d_{kj}^y d_{kj'}^y \right), \end{aligned} \quad (2.40)$$

Note that the potential terms are diagonal in the pseudospectral method. They are represented by their values at the discretized coordinates, so no calculation of potential energy matrix elements is required. The kinetic energy matrices are given by simple analytical expressions (2.39) and (2.40) which can be readily programmed into the computer code. Straightforward programming implementation and high accuracy for moderate number of collocation points constitute the most attractive features of the generalized pseudospectral method.

## 2.4 Numerical solutions of the TDDFT equation

The advantage of time-dependent generalized pseudospectral (TDGPS) procedure

is that it allows nonuniform and optimal spatial grid discretization (denser mesh near each nucleus and sparser mesh at larger electron-nucleus separations). This improves greatly both the accuracy and the efficiency of the electronic structure and time-dependent calculations. For processes such as HHG, accurate time-dependent wave functions are required to achieve convergence since the intensity of various harmonic peaks can span a range of many orders of magnitude.

Consider now the solution of the TDDFT equation recast into the following form:

$$i \frac{\partial}{\partial t} \Psi(\mathbf{r}, t) = \hat{H}(\mathbf{r}, t) \Psi_{i\sigma}(\mathbf{r}, t) = [\hat{H}_0 + \hat{V}(\mathbf{r}, t)] \Psi_{i\sigma}(\mathbf{r}, t) \quad i = 1, 2, \dots, N_\sigma, \quad (2.41)$$

where  $\hat{H}_0$  is the time-independent Hamiltonian, and  $\hat{V}(\mathbf{r}, t)$  includes the electron-laser field interaction and other residual time-dependent terms in

$$\hat{V}(\mathbf{r}, t) = (\mathbf{E}(t) \cdot \mathbf{r}) \sin \omega t + (v_H(\mathbf{r}, t) - v_H(\mathbf{r}, 0)) + (v_{xc,\sigma}(\mathbf{r}, t) - v_{xc,\sigma}(\mathbf{r}, 0)), \quad (2.42)$$

here  $\mathbf{E}(t)$  is the electric field parallel to the internuclear  $z$ -axis, and  $\mathbf{E}(t) = Ff(t)$ , where  $f(t)$  is the envelope function of the laser pulse. We shall extend the second-order split-operator technique in prolate spheroidal coordinates and in the energy representation [33, 34] for the propagation of individual spin-orbital

$$\Psi(\mathbf{r}, t + \Delta t) \cong e^{-i\hat{V}(\mathbf{r}, t)\Delta t/2} e^{-i\hat{H}_0(\mathbf{r})\Delta t} e^{-i\hat{V}(\mathbf{r}, t)\Delta t/2} \Psi(\mathbf{r}, t) + O(\Delta t^3). \quad (2.43)$$

Note that such an expression is different from the conventional split-operator techniques, where  $\hat{H}_0$  is usually chosen to be the kinetic-energy operator and  $\hat{V}$  the remaining Hamiltonian depending on the spatial coordinates only. The use of the energy representation in equation (2.43) allows the explicit elimination of the undesirable fast-oscillating high energy components and speeds up considerably the time propagation.

To pursue the time propagation, we first discretize the Hamiltonian by the GPS method introduced in the last section. Then the wave function on the pseudospectral grid,  $\Psi(\mathbf{r},t)$ , is first propagated according to

$$\Psi'(\mathbf{r},t) = e^{-i\hat{V}(\mathbf{r},t)\Delta t/2}\Psi(\mathbf{r},t), \quad (2.44)$$

since  $e^{-i\hat{V}(\mathbf{r},t)\Delta t/2}$  is a diagonal matrix in the coordinate representation, this is a fast step as far as the CPU time is concerned. To pursue the next step of propagation in the  $\hat{H}_0$  energy space, we construct the time-independent evolution operator

$$e^{-i\hat{H}_0(\mathbf{r})\Delta t} \equiv \hat{S}, \quad (2.45)$$

by means of the GPS discretization and solution of the field free Hamiltonian

$$\hat{H}_0(\xi, \eta)\chi_k(\xi, \eta) = \varepsilon_k\chi_k(\xi, \eta). \quad (2.46)$$

Then the matrix  $S$  can be constructed as

$$S_{ij} \equiv \sum_k \chi_k(\mathbf{r}_i)\chi_k^*(\mathbf{r}_j)e^{-i\varepsilon_k\Delta t}, \quad (2.47)$$

note that  $S$  is a complex symmetric matrix and needs to be constructed only once. Thus the time propagation in the energy space,

$$\Psi''(\mathbf{r},t) = e^{-i\hat{H}_0(\mathbf{r})\Delta t}\Psi'(\mathbf{r},t) = \hat{S}\Psi'(\mathbf{r},t), \quad (2.48)$$

is reduced to the matrix-vector product which can be performed efficiently using the basic linear algebra subroutines. Note that since only a modest number of grid points are required in the present method, and since only half of the grid points in the  $\eta$  coordinate are required for homonuclear diatomic molecules, the overall operation is rather efficient. Finally we perform another fast propagation step similar to that in equation (2.44):

$$\Psi(\mathbf{r},t + \Delta t) = e^{-i\hat{V}(\mathbf{r},t)\Delta t/2}\Psi''(\mathbf{r},t), \quad (2.49)$$

This completes one time propagation step in equation (2.43). After the time-dependent single electron wave functions  $\Psi_{1\sigma}$  are obtained, the total electron density  $\rho(\mathbf{r}, t)$  can be determined.



# Chapter 3

## Optimal control theory

### 3.1 Basic theory

We consider an electron in an external potential  $V(\mathbf{r})$  under the influence of a laser field align in the  $z$ -direction. Given an initial state  $\Psi_{t=0} = \phi_1$ , the time evolution of the wavefunction is described by the time-dependent Schrödinger equation with the laser field modeled in the dipole approximation:

$$i \frac{\partial}{\partial t} \Psi(\mathbf{r}, t) = \hat{H} \Psi(\mathbf{r}, t), \quad (3.1)$$

$$\hat{H} = \hat{H}_0 - \hat{\mu} \varepsilon(t), \quad (3.2)$$

$$\hat{H}_0 = -\frac{\nabla^2}{2} + \hat{V}(\mathbf{r}), \quad (3.3)$$

$\hat{\mu}$  is the dipole operator, and  $\varepsilon(t)$  is the time-dependent electric field.

We want to construct a laser pulse  $\varepsilon(t)$  that drives a quantum system to the final state  $\Psi(T)$  and maximized the expectation value  $J_1$  of an operator  $\hat{O}$  at the end of the external field:

$$J_1[\Psi] = \frac{1}{T} \int_0^T \langle \Psi(t) | \hat{O} | \Psi(t) \rangle dt, \quad (3.4)$$

The target operator  $\hat{O}$  is restricted to be a Hermitian operator, and it can be consistent with two parts

$$\hat{O}(t) = 2T\delta(t-T)\hat{O}_1 + \hat{O}_2(t), \quad (3.5)$$



$\hat{O}_1$  is the final-time target operator, and  $\hat{O}_2$  is the time-dependent target operator.

In addition to the maximization of  $J_1[\Psi]$ , we require that the fluence of the laser field be as small as possible to avoid irrational solutions and it is cast in the following form:

$$J_2[\varepsilon] = -\alpha \int_0^T [\varepsilon(t)]^2 dt, \quad (3.6)$$

$\alpha$  is a positive small constant which play the role of penalty factors, and high laser fluence will cause more negative the expression. The penalty factor can be extended to a time-dependent function  $\alpha(t)$  to enforce a given time-dependent shape of the laser pulse, e.g. a Gaussian or sinusoidal envelope.

The constraint that the electronic wavefunction has to propagate with the time-dependent Schrödinger equation (TDSE) is expressed by[35, 36]

$$J_3[\Psi, \varepsilon, \chi] = -2Im \int_0^T \left\langle \chi(t) \left| i \frac{\partial}{\partial t} - \hat{H}(t) \right| \Psi(t) \right\rangle dt, \quad (3.7)$$

Here we have introduced the Lagrange multiplier  $\chi(t)$ . Since we require the TDSE to be satisfied by the complex conjugate of the wavefunction as well, we obtain the imaginary part of the functional.

The Lagrange functional has the form

$$J[\Psi, \varepsilon, \chi] = J_1[\Psi] + J_2[\varepsilon] + J_3[\Psi, \varepsilon, \chi], \quad (3.8)$$

We refer to this functional as the standard optimal control problem and start the discussion of all extensions considered in this work from this standard form.

To find the optimal laser field from the functional in equation (3.8) we perform a total variation. Since the variables  $\Psi$ ,  $\chi$  and  $\varepsilon$  are linearly independent we can treat them individually. We have omitted the derivations with respect to the complex

conjugate of the wavefunction  $\Psi^*(t)$  and the Lagrange multiplier  $\chi^*(t)$ , since the functional derivative will result in the complex conjugate equations for these variations.

The necessary condition for a maximum of J is

$$\delta J = 0 \rightarrow \delta_{\Psi} J = 0, \quad \delta_{\varepsilon} J = 0, \quad \delta_{\chi} J = 0. \quad (3.9)$$

The functional derivative of J with respect to  $\Psi$

$$\delta_{\Psi} J = \int_0^T d\tau \left\{ \frac{1}{T} \langle \Psi(\tau) | \hat{O} | \delta \Psi(\tau) \rangle + i \left\langle \left( i \frac{\partial}{\partial \tau} - \hat{H}(\tau) \right) \chi(\tau) | \delta \Psi(\tau) \right\rangle \right\} - \langle \chi(T) | \delta \Psi(T) \rangle + \langle \chi(0) | \delta \Psi(0) \rangle, \quad (3.10)$$

The variation of  $\delta \Psi(0)$  vanishes because we have a fixed initial condition,  $\Psi(0) = \phi_1$ .

Then it's the variation of J with respect to  $\chi$ , and in contrast to the variation with respect to  $\Psi$  we do not have boundary terms here

$$\delta_{\chi} J = -i \int_0^T d\tau \left\langle \left( i \frac{\partial}{\partial \tau} - \hat{H}(\tau) \right) \Psi(\tau) | \delta \chi(\tau) \right\rangle, \quad (3.11)$$

Finally, the variation with respect to  $\varepsilon(t)$  yields

$$\delta_{\varepsilon} J = \int_0^T d\tau \{ -2\alpha\varepsilon(\tau) - 2 \text{Im} \langle \chi(\tau) | \hat{\mu} | \Psi(\tau) \rangle \} \delta \varepsilon, \quad (3.12)$$

Setting each of the variations independently to zero will result in the desired control equations.

## 3.2 Final-time targets and algorithms

In this section we introduce the scheme to solve the optimal control theory with final-time target[22]. From  $\delta_{\varepsilon} J = 0$  we find

$$\alpha\varepsilon(t) = -\text{Im} \langle \chi(t) | \hat{\mu} | \Psi(t) \rangle. \quad (3.13)$$

The laser field  $\varepsilon(t)$  is calculated from the wavefunction  $\Psi(t)$  and the Lagrange multiplier

$\chi(t)$  at the same point in time. The variation  $\delta_\chi J$  in equation (3.11) yields a time-dependent Schrödinger equation for  $\Psi(t)$  with a fixed initial state  $\phi_i$ ,

$$(i \frac{\partial}{\partial t} - \hat{H}(t))\Psi(\mathbf{r}, t) = 0, \quad \Psi(\mathbf{r}, 0) = \phi_i \quad (3.14)$$

Note that this equation also depends on the laser field  $\varepsilon(t)$  via the Hamiltonian.

The variation with respect to the wavefunction  $\delta_\Psi J$  results in

$$(i \frac{\partial}{\partial t} - \hat{H}(t))\chi(\mathbf{r}, t) = i(\chi(\mathbf{r}, t) - \hat{O}_1 \Psi(\mathbf{r}, t))\delta(t - T), \quad (3.15)$$

if we require the Lagrange multiplier  $\chi(t)$  to be continuous at  $t = T$ , we can solve the following two equations instead of equation we integrate over equation

$$(i \frac{\partial}{\partial t} - \hat{H}(t))\chi(\mathbf{r}, t) = 0, \quad (3.16)$$

$$\chi(\mathbf{r}, T) = \hat{O}_1 \Psi(\mathbf{r}, T). \quad (3.17)$$

To show this we integrate over equation

$$\lim_{\kappa \rightarrow 0} \int_{T-\kappa}^{T+\kappa} dt (i \frac{\partial}{\partial t} - \hat{H}(t))\chi(\mathbf{r}, t) = \lim_{\kappa \rightarrow 0} \int_{T-\kappa}^{T+\kappa} dt i(\chi(\mathbf{r}, t) - \hat{O}_1 \Psi(\mathbf{r}, t))\delta(t - T), \quad (3.18)$$

the left-hand side vanishes because the integrand is a continuous function. It follows that also the right-hand side must vanish, which implies equation(3.17). From equations (3.17) and (3.15) then follows equation (3.16). Hence, the Lagrange multiplier  $\chi(t)$  satisfies a time-dependent Schrödinger equation with an initial condition at  $t = T$ .

In the following, we present the standard approaches to solve the optimal control problem[37]. As the word iterative already indicates, it will be necessary to solve the time-dependent Schrödinger equation more than once. Even with the present computational resources this limits the application of the algorithms to relatively low-dimensional systems.

The scheme starts with propagating  $\phi_1 = \Psi_0(0)$  forward in time. After the initial propagation we determine the final state for the Lagrange multiplier wavefunction  $\chi_0(T)$  by applying the target operator to the final state of the wavefunction  $\hat{O}_1 \Psi_0(T)$ . The laser field for the backward propagation for  $\chi_0(t)$ ,  $\tilde{\varepsilon}(t)$  is determined by

$$\tilde{\varepsilon}(t) = -\frac{1}{\alpha} \text{Im} \langle \chi_k(t) | \hat{\mu} | \Psi_k(t) \rangle \quad (3.19)$$

The propagation from  $\chi_0(T)$  to  $\chi_0(T - dt)$  is done with the field  $\tilde{\varepsilon}_0(T)$ , where we use  $\chi_0(T)$  and  $\Psi_0(T)$  in equation (3.19). The small error introduced here is compensated by choosing a sufficiently small time step. In parallel, we propagate  $\Psi_0(T)$  backward with the previous field  $\varepsilon_0(t)$ . This additional parallel propagation is only necessary if the storage of  $\Psi_0(t)$  in the memory is not possible. For the next propagation step from  $\chi_0(T - dt)$  to  $\chi_0(T - 2dt)$  we use  $\Psi_0(T - dt)$  and  $\chi_0(T - dt)$  in equation (3.19). We repeat these steps until  $\chi_0(0)$  is reached. We summarize the whole iteration step by

$$\begin{aligned} [\Psi_k(T) &\xrightarrow{\varepsilon_k(t)} \Psi_k(0)] \\ \hat{O} \Psi_k(T) = \chi_k(T) &\xrightarrow{\tilde{\varepsilon}_k(t)} \chi_k(0) \end{aligned} \quad (3.20)$$

The last part of the zeroth iteration step consists in setting  $\Psi_1(0) = \phi_1$  and propagating  $\Psi_1(0)$  forward with the field  $\varepsilon_1(t)$  determined by

$$\varepsilon_{k+1}(t) = -\frac{1}{\alpha} \text{Im} \langle \chi_k(t) | \hat{\mu} | \Psi_{k+1}(t) \rangle \quad (3.21)$$

This completes the zeroth iteration step. The loop is closed by continuing with equation (3.20).

If the initial guess for the laser field is appropriate the algorithm starts converging very rapidly and in a monotonic way, meaning that the value for the functional  $J$  in equation (3.8) is increasing at each iteration step. The monotonic convergence can be proven analytically. In the proof an infinitely accurate solution of the time-dependent

Schrödinger equation is assumed. Since this is not possible in practice, it may happen that the functional decreases in the numerical scheme, e.g., when absorbing boundaries are employed. This sensitivity provides an additional check on the accuracy of the propagation.

### 3.3 Time-dependent targets and algorithms

In this section, we deal with the time dependent targets [38, 39]. The control equations are the same as last section except the variation respect to  $\Psi$ ,

$$(i\frac{\partial}{\partial t} - \hat{H}(t))\chi(r,t) = -\frac{1}{T}\hat{O}_2\Psi(r,t), \quad \chi(\vec{r},T) = 0. \quad (3.22)$$

Its solution can be formally written as

$$\chi(\mathbf{r},t) = \hat{U}_0^t \chi(\mathbf{r},0) - \frac{1}{T} \int_0^t d\tau \hat{U}_\tau^t [\hat{O}_2(\tau)\Psi(\mathbf{r},t)]. \quad (3.23)$$

where  $\hat{U}_0^t$  is the time-evolution operator defined by

$$\hat{U}_0^t = \mathcal{T} \exp\left[-i \int_0^t dt' \hat{H}(t')\right]. \quad (3.24)$$

with the time-ordering operator  $\mathcal{T}$ .

Equipped with the control equations (3.13), (3.14), (3.22) we have to find an algorithm to solve these equations for  $\varepsilon(t)$ . In the following, we describe such a scheme which is similar to last section. The additional parameters  $\eta$  and  $\xi$  have been ‘artificially’ introduced (not derived by a functional variation) to ‘fine tune’ the convergence of the algorithm. A monotonic convergence in  $J$  can be proven if  $\eta \in [0, 1]$  and  $\xi \in [0, 2]$ . Here,  $\alpha$  is always the penalty factor.

The algorithm starts with propagating  $\Psi_0(0) = \phi_i$  forward in time with an initial guess for the laser field  $\varepsilon_0(t)$ . The backward propagation of  $\chi_0(t)$  is started from  $\chi_0(T) = 0$  solving an inhomogeneous time-dependent Schrödinger equation which requires  $\Psi_0(t)$  as input,

$$\begin{aligned} [\Psi_k(T) &\rightarrow \varepsilon_k(t) \rightarrow \Psi_k(0)] \\ \chi_k(T) = 0 &\rightarrow \tilde{\varepsilon}_k(t), \Psi_k(t) \rightarrow \chi_k(0), \end{aligned} \quad (3.25)$$

The brackets indicate that the storage of the wavefunction  $\Psi_0(t)$  can be avoided if we propagate it backwards in time as well using  $\varepsilon_0(t)$ . The backward propagation of  $\chi_0(t)$  requires the laser field determined by,

$$\tilde{\varepsilon}_k(t) = (1 - \eta)\varepsilon_k(t) - \frac{\eta}{\alpha} \text{Im} \langle \chi_k(t) | \hat{\mu} | \Psi_k(t) \rangle. \quad (3.26)$$

The next step is to start a forward propagation of  $\Psi_1(0) = \phi_1$

$$\begin{aligned} [\chi_k(0) &\rightarrow \tilde{\varepsilon}_k(t), \Psi_k(t) \rightarrow \chi_k(T)] \\ [\Psi_k(0) &\rightarrow \varepsilon_k(t) \rightarrow \Psi_k(T)], \\ \Psi_{k+1}(0) &\rightarrow \varepsilon_{k+1}(t) \rightarrow \Psi_{k+1}(T) \end{aligned} \quad (3.27)$$

and calculate the laser field

$$\varepsilon_{k+1}(t) = (1 - \gamma)\tilde{\varepsilon}_k(t) - \frac{\gamma}{\alpha} \text{Im} \langle \chi_k(t) | \hat{\mu} | \Psi_{k+1}(t) \rangle. \quad (3.28)$$

If we want to avoid storing  $\chi_0(t)$  in the memory we have to perform an additional forward propagation which in turn requires the knowledge of  $\Psi_0(t)$ . These extra propagations are indicated by the expressions in brackets. After the time evolution is complete we can close the loop and continue with equation (3.25).

### 3.4 Conjugate gradient method

Here we outline the concept of the conjugate gradient method.

The gradient at the k-th iteration can be evaluated by the expression

$$g_k(t) \equiv \frac{\delta J}{\delta \varepsilon_k} = -\frac{1}{\alpha} \text{Im} \langle \chi_k(t) | \hat{\mu} | \Psi_k(t) \rangle. \quad (3.29)$$

To search for an optimal field, one may invoke Polak-Ribière-Polyak search direction as follows

$$d_k(t_i) = g_k(t_i) + \eta_k d_{k-1}(t_i), \quad i = 1, 2, \dots, N, \quad k = 1, 2, \dots, \quad (3.30)$$

where the starting direction is

$$d_0(t_i) = g_0(t_i), \quad i = 1, 2, \dots, N, \quad (3.31)$$

which is the gradient corresponding to the initial laser field  $\varepsilon_0(t)$ , the conjugate gradient update parameter

$$\eta_k = \frac{\mathbf{g}_k^{Tran} (\mathbf{g}_k - \mathbf{g}_{k-1})}{\mathbf{g}_{k-1}^T \mathbf{g}_{k-1}}, \quad (3.32)$$

with *Tran* denoting the vector transpose and  $\mathbf{g}_k^{Tran} = (\mathbf{g}_k(t_1), \mathbf{g}_k(t_2), \dots, \mathbf{g}_k(t_n))$ , the transpose of the vector  $\mathbf{g}_k$  due to the discretization of the time interval  $[0, T]$  into  $N$  slices. The time-dependent laser field  $\varepsilon(t)$  is updated according to

$$\varepsilon_{k+1}(t_i) = \varepsilon_k(t_i) + \lambda d_k(t_i), \quad i = 1, 2, \dots, N, \quad (3.33)$$

The constant  $\lambda_s$  is a step length that maximizes the cost functional  $J[\varepsilon_{k+1}]$  (for the  $(k + 1)$ -th iteration) and can be determined by a line search at each direction.

### 3.5 Constraints on the optimal fields

The optimized laser field directly obtained by the iterative scheme usually filled with very high frequency and unrealistic behavior signals. Thus we shall take further restrictions on the optimal field to derive the results in better sense. But these constraints have to put into scheme carefully, the monotonic convergence is not guaranteed here after the implementation of them.

#### *Fluence constraint*

In order to fix the fluence of the optimized laser pulse to a given value  $E_0$ , we have to replace the functional  $J_2$  by

$$\tilde{J}_2 = \alpha \left[ \int_0^T dt \varepsilon(t)^2 - E_0 \right]. \quad (3.34)$$

Here  $\alpha$  is a Lagrange multiplier. We have to vary with respect to it when calculating the total variation of  $J$ . The variation with respect to  $\alpha$  results in an additional equation

$$\int_0^T dt \varepsilon(t)^2 = E_0. \quad (3.35)$$

In the case where  $\alpha$  is a penalty factor its value has to be set externally, while here the

additional equation can be rewritten [40] to determine the value of the Lagrange multiplier  $\alpha$ .

Inserting equation (3.13) into equation (3.35) yields

$$\begin{aligned} \frac{1}{\alpha^2} \int_0^T dt [\text{Im} \langle \chi(t) | \hat{\mu} | \Psi(t) \rangle]^2 &= E_0 \\ \Rightarrow \alpha &= \sqrt{\int_0^T dt [\text{Im} \langle \chi(t) | \hat{\mu} | \Psi(t) \rangle]^2 / E_0}. \end{aligned} \quad (3.36)$$

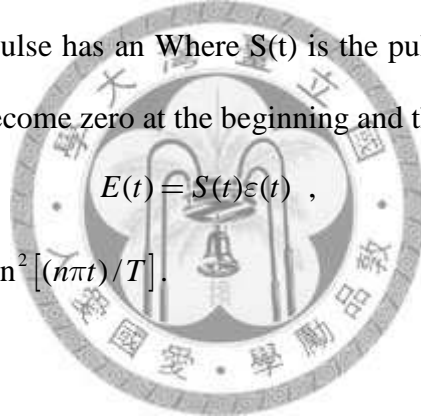
The remaining part of the functional stays the same, so the variations do not change, and we keep the control equations: (3.13), (3.14), (3.16), and (3.17)

### *Laser-envelope constraints*

If we want the laser pulse has an envelope function  $S(t)$  is the pulse envelope function and is to force the laser field to become zero at the beginning and the end of the pulse

$$E(t) = S(t)\varepsilon(t), \quad (3.37)$$

,for example:  $S(t) = \sin^2[(n\pi t)/T]$ .



### *Spectral constraints*

If spectral filtering is required, we formulate the constraint with the help of a filter function  $h(\omega)$ , the Fourier transform  $F$  and its inverse  $F^{-1}$

$$\tilde{\varepsilon}_k(t) = F^{-1}[h(\omega)F[\varepsilon_k(t)]], \quad (3.38)$$

$h(\omega)$  is a filter function, for example

$$h(\omega) = \left\{ \left[ 1 + \left( \frac{\omega_l}{\omega} \right)^{2n} \right] \left[ 1 + \left( \frac{\omega}{\omega_h} \right)^{2n} \right] \right\}^{-1/2}, \quad (3.39)$$

Which is the Butterworth bandpass filter with  $\omega_l$  and  $\omega_h$  being the low and high cutoff frequencies (e.g., corresponding to a Ti: sapphire laser of the wavelength around 800 nm, the pulse duration between 100 and a few femtoseconds).



# Chapter 4

## Results and discussion

### 4.1 Orbital energies

Table I (A) Spin orbital energies of diatomic molecules of present DFT calculations with  $LB_u$  potential(a.u.). (B) Experimental vertical ionization potentials(a.u.).

Molecule	Bond length	Orbital	Ion state A	B[41-43]	
N <sub>2</sub>	2.072	1 $\sigma_g$		-14.7951	-15.0492
		1 $\sigma_u$		-14.7939	-15.0492
		2 $\sigma_g$		-1.2153	-1.3708
		2 $\sigma_u$		-0.6778	-0.6883
		1 $\pi_u$		-0.6190	-0.6233
		3 $\sigma_g$		-0.5675	-0.5726
		CO	2.132	1 $\sigma$	
2 $\sigma$				-10.6548	-10.8742
3 $\sigma$				-1.2544	-1.3964
4 $\sigma$				-0.7066	-0.7239
1 $\pi$				-0.6270	-0.6247
5 $\sigma$				-0.5082	-0.5144
O <sub>2</sub>	2.287			2 $\sigma_u\uparrow$	$^2\Sigma_u^-$
		2 $\sigma_u\downarrow$	$^4\Sigma_u^-$	-0.8809	-0.9029
		3 $\sigma_g\uparrow$	$^2\Sigma_g^-$	-0.7210	-0.7463
		3 $\sigma_g\downarrow$	$^4\Sigma_g^-$	-0.7192	-0.6680
		1 $\pi_u\uparrow$	$^2\Pi_u$	-0.6667	-0.6485
		1 $\pi_u\downarrow$	$^4\Pi_u$	-0.6307	-0.6140
		1 $\pi_g\uparrow$	$^2\Pi_g$	-0.4799	-0.4522

The ground-state electronic configurations of  $N_2$ , CO, and  $O_2$  are  $1\sigma_g^2 1\sigma_u^2 2\sigma_g^2 2\sigma_u^2 1\pi_u^4 3\sigma_g^2$ ,  $1\sigma^2 2\sigma^2 3\sigma^2 4\sigma^2 1\pi^2 5\sigma^2$ , and  $1\sigma_g^2 1\sigma_u^2 2\sigma_g^2 2\sigma_u^2 3\sigma_g^2 1\pi_u^4 1\pi_g^4$ , respectively.

In Table I, we summarize the energies for the spin orbitals that have a significant contribution to MPI and the corresponding experimental vertical ionization potentials. While  $N_2$  and CO represent the spin compensated case with the same orbital energies for both spin projections,  $O_2$  is a spin-polarized system where the spin orbital energies depend on the spin. With the correction of long range behavior of the coulomb potential, the agreement between the calculated and experimental values is fairly good, particularly for  $N_2$  and CO molecules.

The CO molecule was unequal nuclear charges, and its ground electronic state has a permanent dipole moment about 0.112 Debye. Also the inversion symmetry of the potential is broken. This will cause the Stark effect, and the HOMO energy shift significantly from its unperturbed value. The  $N_2$  and  $O_2$  molecules are symmetric with respect to inversion, thus the Stark shift is quadratic in the field strength and its value is quite small. Here, we performed the self-consistent DFT calculations of  $N_2$  and CO in the field parallel to the molecular axis to estimate how large the Stark shift changes the ionization potential.

The field strength is 0.01195 a.u. which corresponds to the intensity  $5 \times 10^{12} \text{W/cm}^2$ . From Table II, we can see the shift of the HOMO energy in CO molecule is large even in the field as weak as  $5 \times 10^{12} \text{W/cm}^2$ .

Table II HOMO energies of  $N_2$  and CO molecules in DC electric field(positive field direction is from C to O)

Electric field(a.u.)	HOMO energy of $N_2$ (a.u.)	HOMO energy of CO(a.u.)
-1.195E-02	-0.5672	-0.4971
0	-0.5675	-0.5082
1.195E-02	-0.5672	-0.5198

## 4.2 Multiphoton ionization

Once the time-dependent wave functions and therefore the time-dependent electron densities are obtained, we can calculate the time-dependent multiphoton ionization probability of an individual spin-orbital according to

$$P_{i,\sigma} = 1 - N_{i,\sigma}(t), \quad (4.1)$$

where

$$N_{i,\sigma}(t) = \langle \Psi_{i,\sigma}(t) | \Psi_{i,\sigma}(t) \rangle, \quad (4.2)$$

is the time-dependent population (survival probability) of the  $i\sigma$ -th spin-orbital.

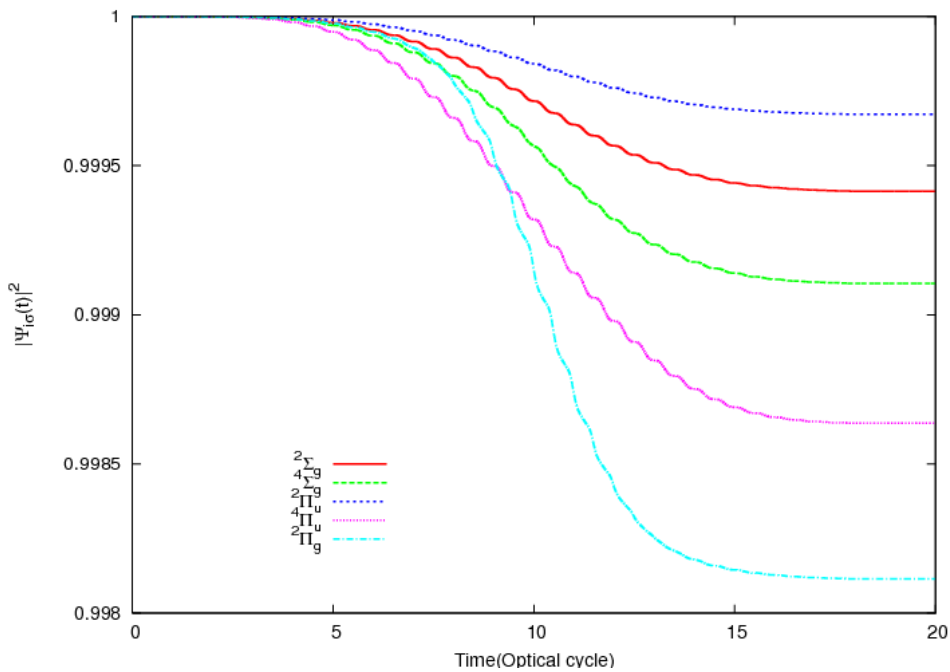
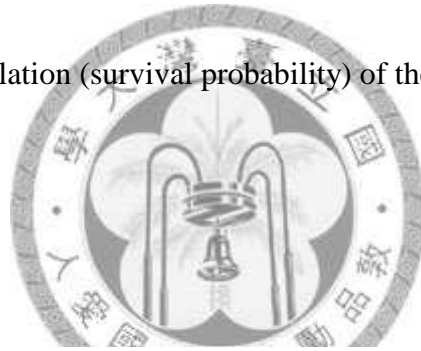


Figure 4-1 The time-dependent population of electrons of individual spin orbitals of  $O_2$  in 20-optical-cycle, 800 nm,  $\sin^2$  laser pulses. The laser intensities is  $10^{14} \text{ W/cm}^2$

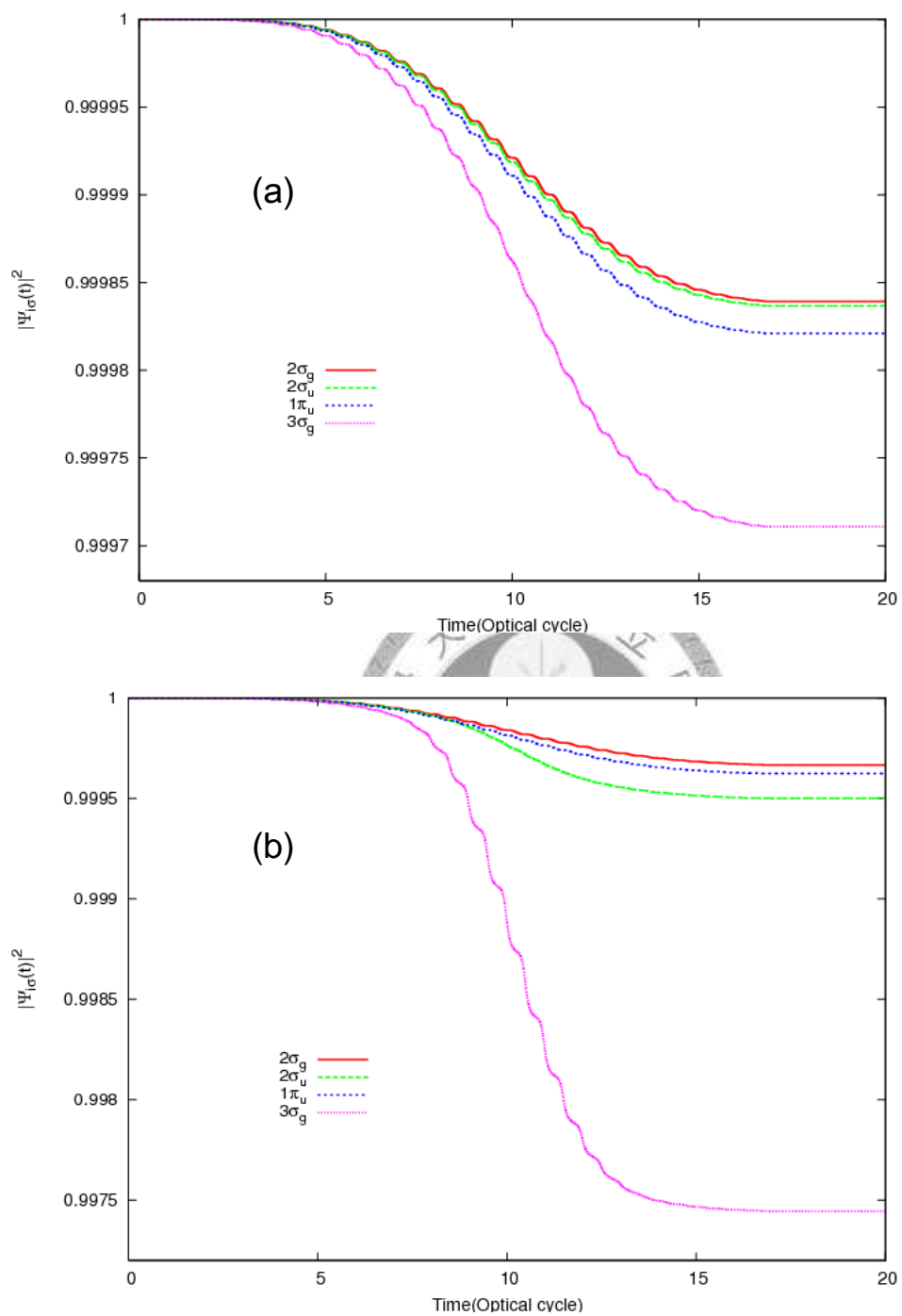


Figure 4-2 The time-dependent population of electrons of individual spin orbitals of  $N_2$  in 20-optical-cycle, 800 nm,  $\sin^2$  laser pulses. The laser intensities are (a)  $5 \times 10^{13}$ , (b)  $10^{14}$   $W/cm^2$

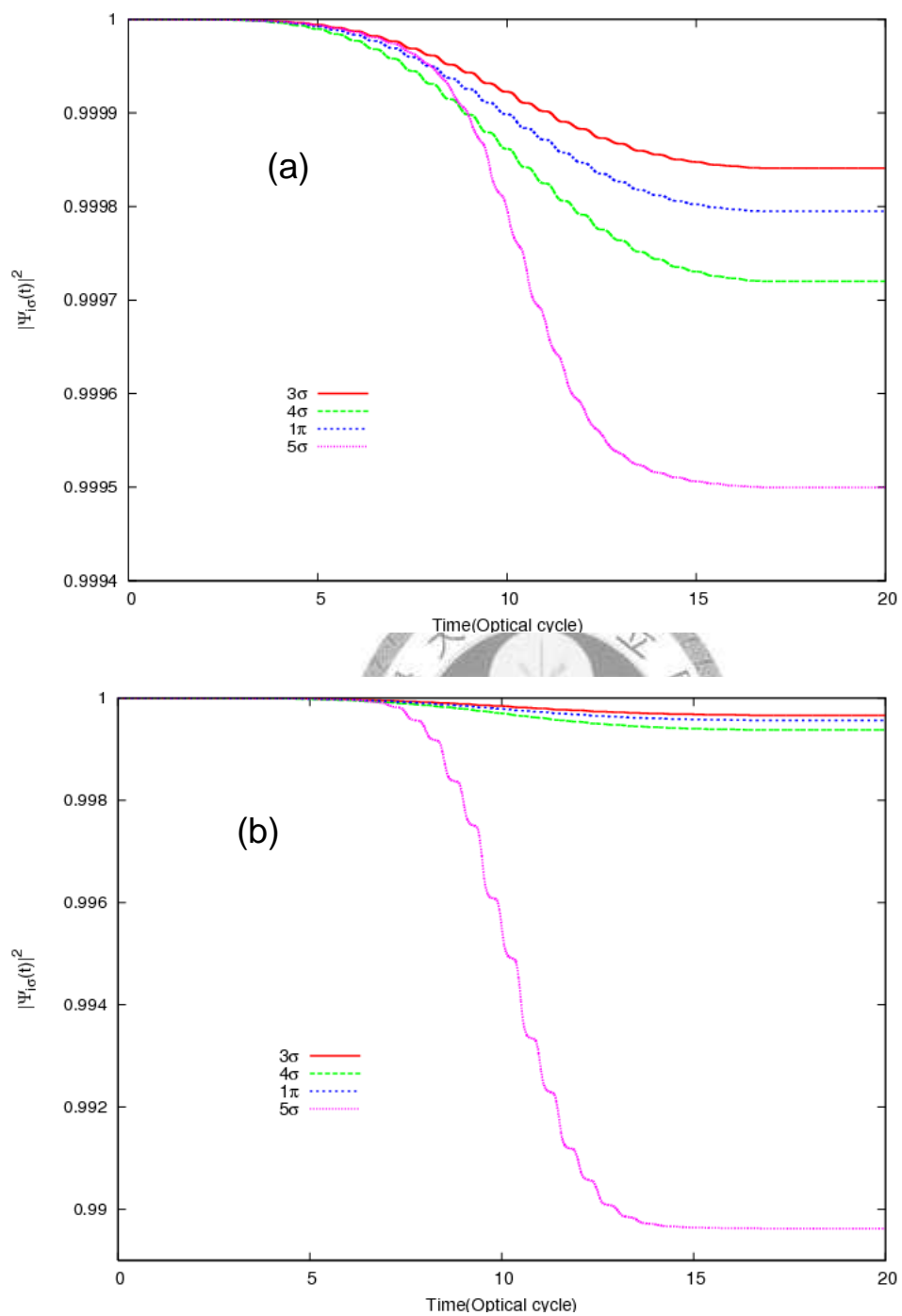


Figure 4-3 The time-dependent population of electrons of individual spin orbitals of CO in 20-optical-cycle, 800 nm,  $\sin^2$  laser pulses. The laser intensities are (a)  $5 \times 10^{13}$ , (b)  $10^{14} \text{ W/cm}^2$

In Figure 4-1~Figure 4-3, we can see the order of the ionization probability of each orbital is not totally dependent on their ionization potential. For example in Figure 4-2 (b), although  $1\pi_u$  has lower ionization potential than  $2\sigma_u$ , the ionization probability of the  $1\pi_u$  electrons turns out to be less than that of the  $2\sigma_u$  electrons. However if we arrange  $\sigma$  and  $\pi$  orbitals individually, orbitals have lower ionization potential always ionize more. This may be attributed to the fact that  $2\sigma_u$  orbital is along the electric-field direction, while that of  $1\pi_u$  is perpendicular to it. We thus observe two different effects that contribute to the ionization: the ionization potential (electron binding energy) effect and the orbital orientation effect. The ionization potential effect makes the electrons with lower ionization potentials easier to ionize. The orientation effect makes the ionization easier for those electrons whose orbital orientations are parallel to the electric field. These two effects are clearly competing.

The multiphoton ionization occurs mainly in the tunneling regime in intense low-frequency laser fields. The probability of the tunneling ionization is very sensitive with respect to the HOMO energy. From last section, we know that the Stark effect will shift the energy potential of the CO molecule largely. Thus we can observe the ionization probability of CO molecules is much larger than that of  $N_2$  and  $O_2$

### 4.3 High-order harmonic generation

The time-dependent induced dipole moment can now be calculated as

$$d(t) = \int z\rho(\mathbf{r},t)d\mathbf{r} = \sum_{i\sigma} d_{i\sigma}(t) \quad (4.3)$$

where

$$d_{i\sigma}(t) = n_{i\sigma} \langle \Psi_{i\sigma}(\mathbf{r},t) | z | \Psi_{i\sigma}(\mathbf{r},t) \rangle \quad (4.4)$$

Is the induced dipole moment of the  $i\sigma$ -th spin-orbital. The corresponding HHG power spectrum may now be obtained by the Fourier transfer of the respective time-dependent dipole moment

$$P(\omega) = \left| \frac{1}{t_f - t_i} \int_{t_i}^{t_f} d(t) e^{-i\omega t} dt \right|^2 \quad (4.5)$$

In

Figure 4-4, we present the high-order harmonic generation power spectrum of  $N_2$ ,  $CO$ , and  $O_2$ . The cutoff regime in the  $N_2$  and  $O_2$  molecules is clearly shown and increase as the field grow stronger. The most notable feature of the spectrum of the  $CO$  molecule is existence of both odd and even harmonics while others only generate odd-order harmonics. In an earlier study, even-order harmonics can be produced only by means of the breakdown of the Born-Oppenheimer approximation.

From Figure 4-5 to Figure 4-10, we show the induced dipole moment and HHG power spectrum of several orbitals. We can see the HOMO is the dominant contribution to the total HHG power spectrum, but the calculations of inner electrons also have to be included for the accurate and detailed results.

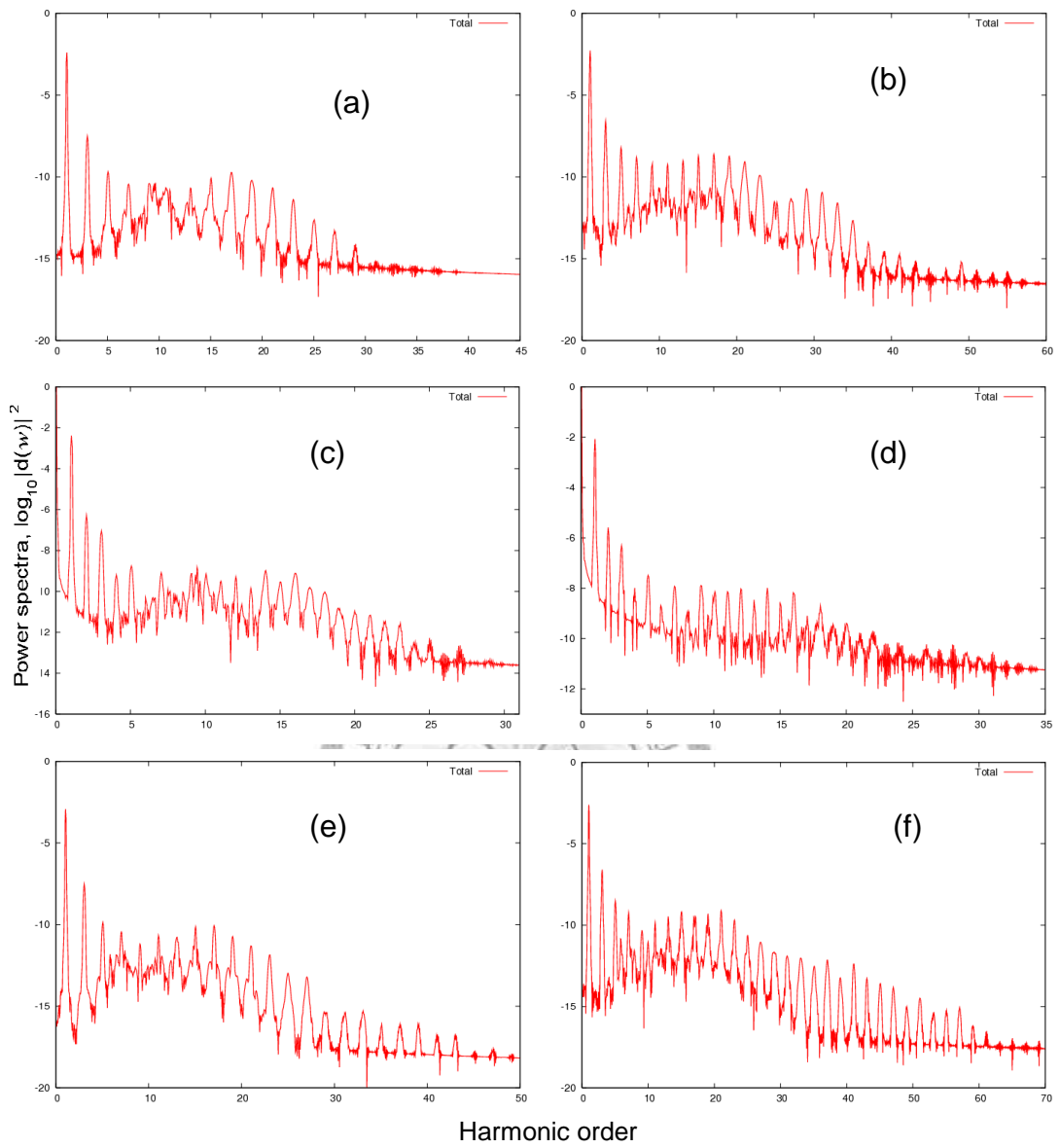


Figure 4-4 The HHG power spectrum of  $N_2$  in the field intensity (a)  $5 \times 10^{13} \text{ W/cm}^2$  and (b)  $10^{14} \text{ W/cm}^2$ , of CO in the field intensity (c)  $5 \times 10^{13} \text{ W/cm}^2$  and (d)  $10^{14} \text{ W/cm}^2$ , and of  $O_2$  in the field intensity (e)  $5 \times 10^{13} \text{ W/cm}^2$  and (f)  $10^{14} \text{ W/cm}^2$ , 800nm,  $\sin^2$  laser pulses.



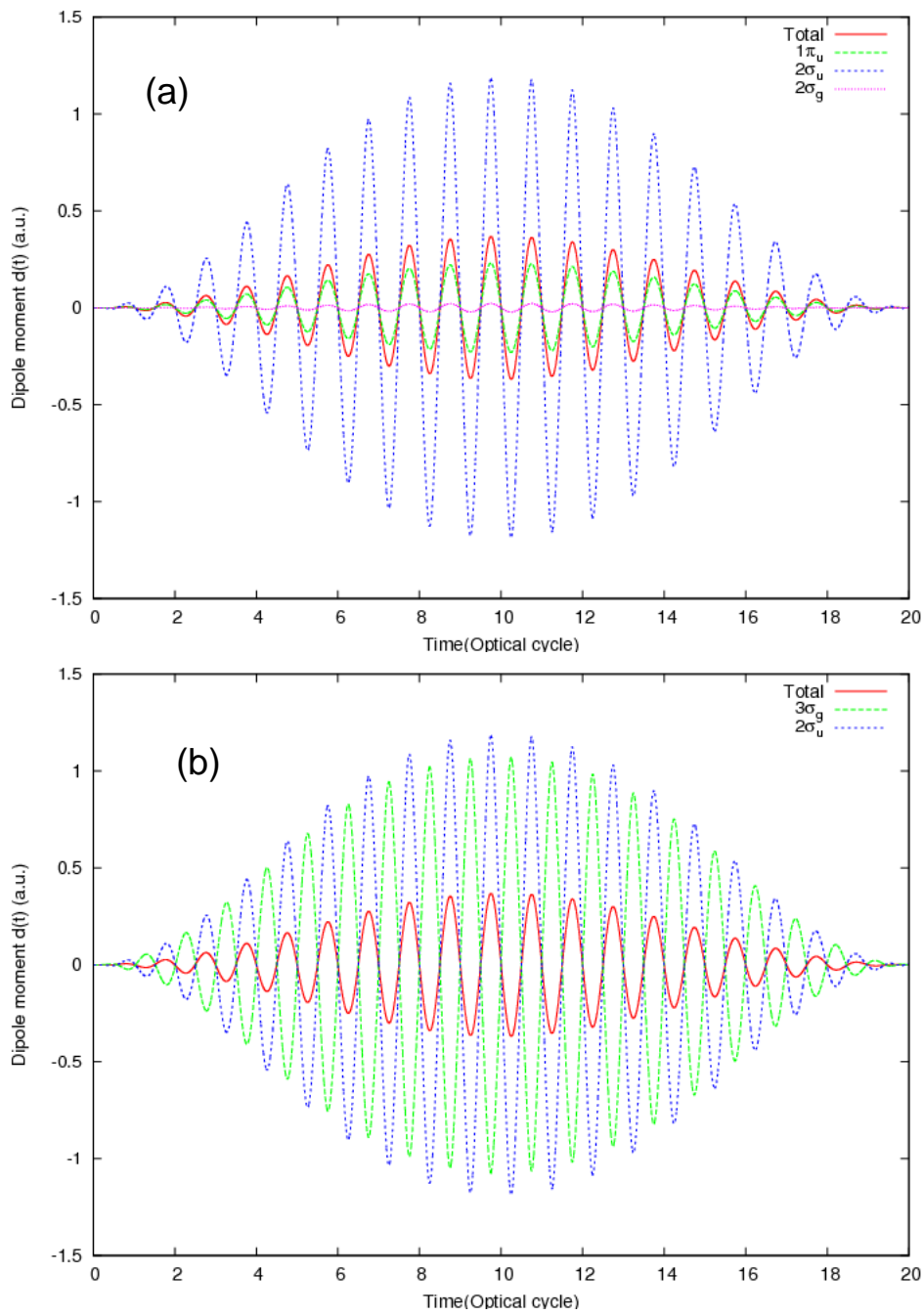


Figure 4-5 Comparison of the induced dipole moment of  $N_2$  from different spin orbital in  $10^{14}$  W/cm<sup>2</sup>, 800nm,  $\sin^2$  laser pulses

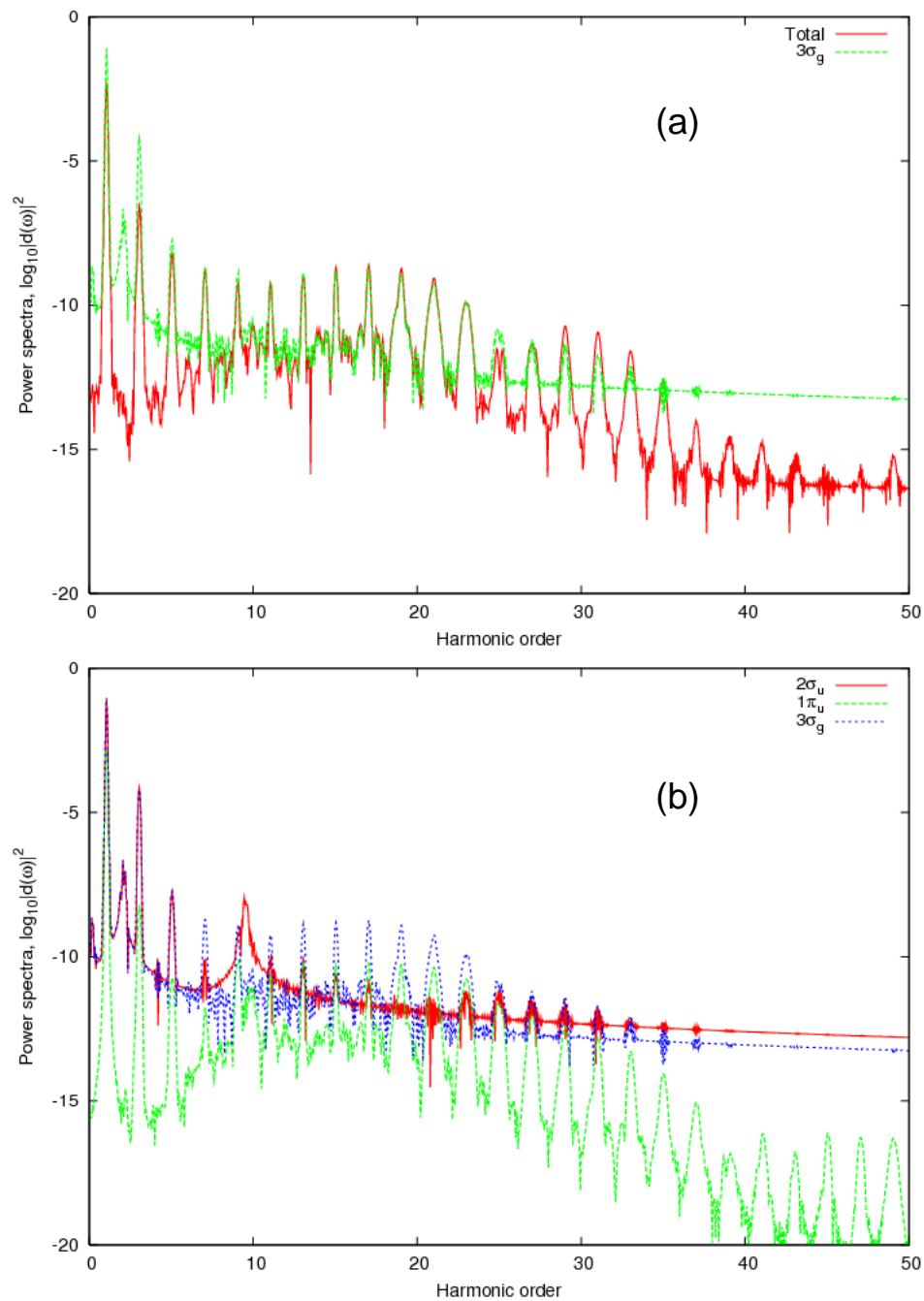


Figure 4-6 (a) Comparison of the total HHG power spectrum and the partial contributions from HOMO of  $N_2$ , and (b) from different spin orbital in  $10^{14} \text{ W/cm}^2$ , 800nm,  $\sin^2$  laser pulses

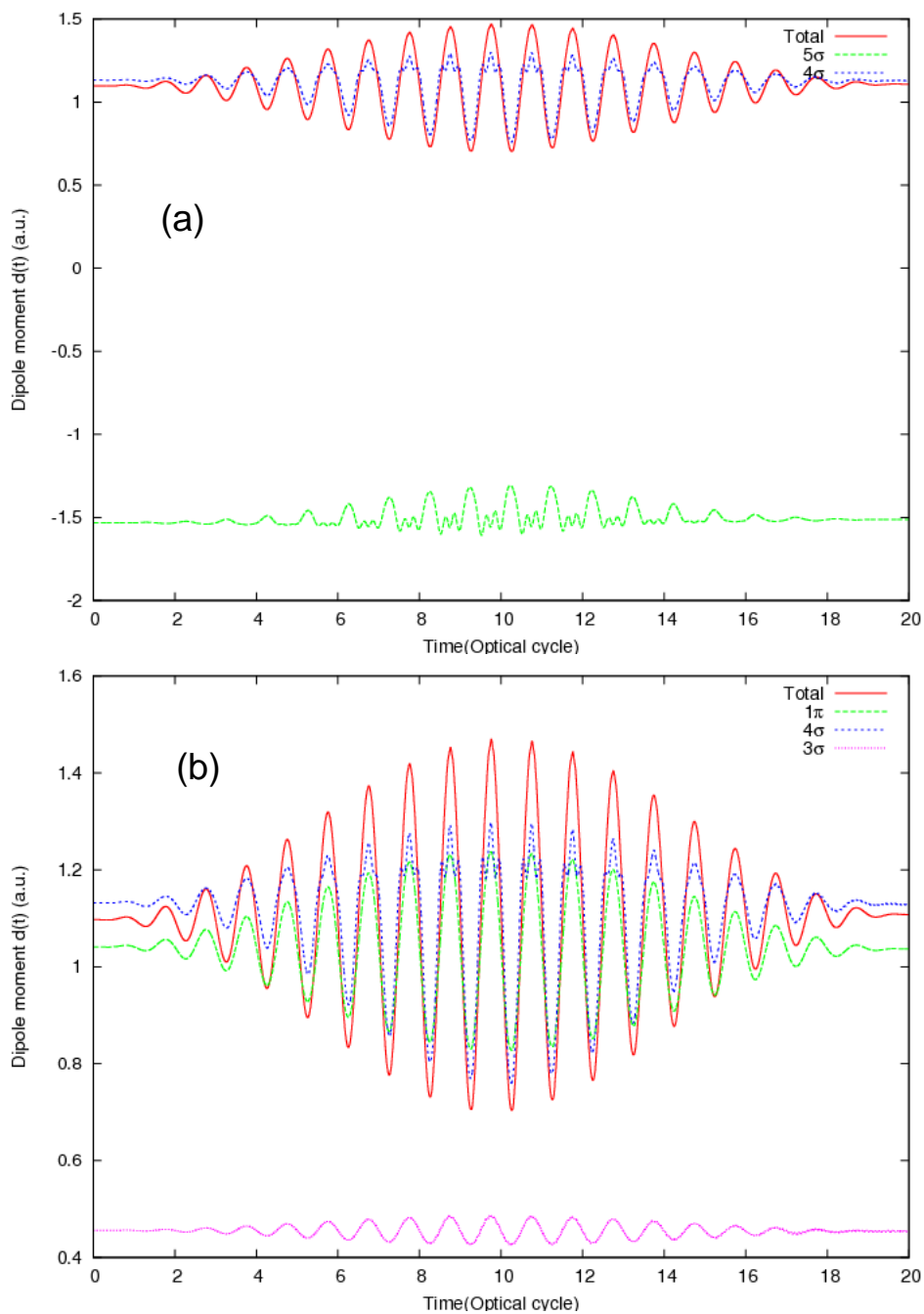


Figure 4-7 Comparison of the induced dipole moment of CO from different spin orbital in  $10^{14} \text{ W/cm}^2$ ,  $800 \text{ nm}$ ,  $\sin^2$  laser pulses

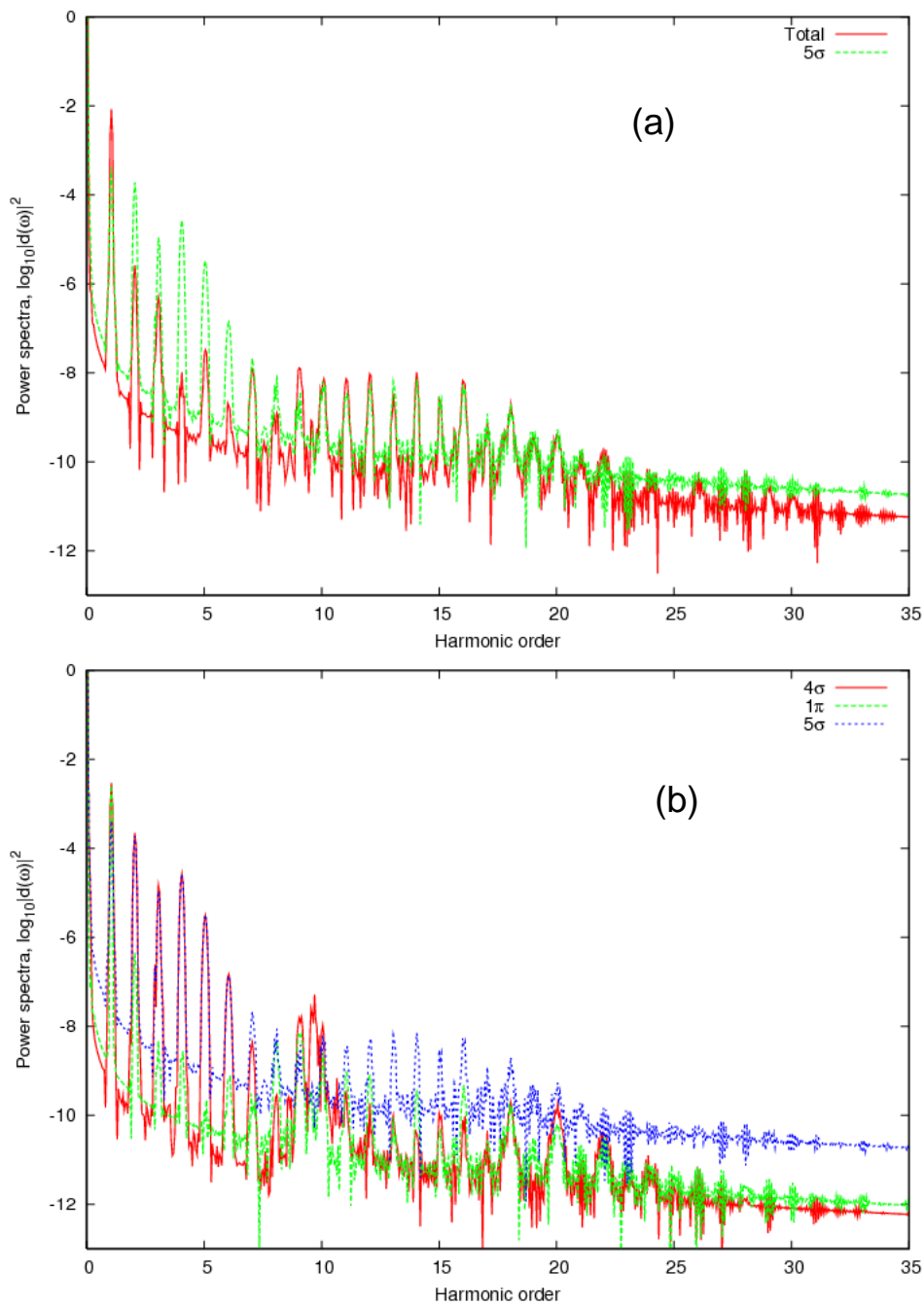


Figure 4-8 (a) Comparison of the total HHG power spectrum and the partial contributions from HOMO of CO, and (b) from different spin orbital in  $10^{14}$  W/cm<sup>2</sup>, 800nm,  $\sin^2$  laser pulses

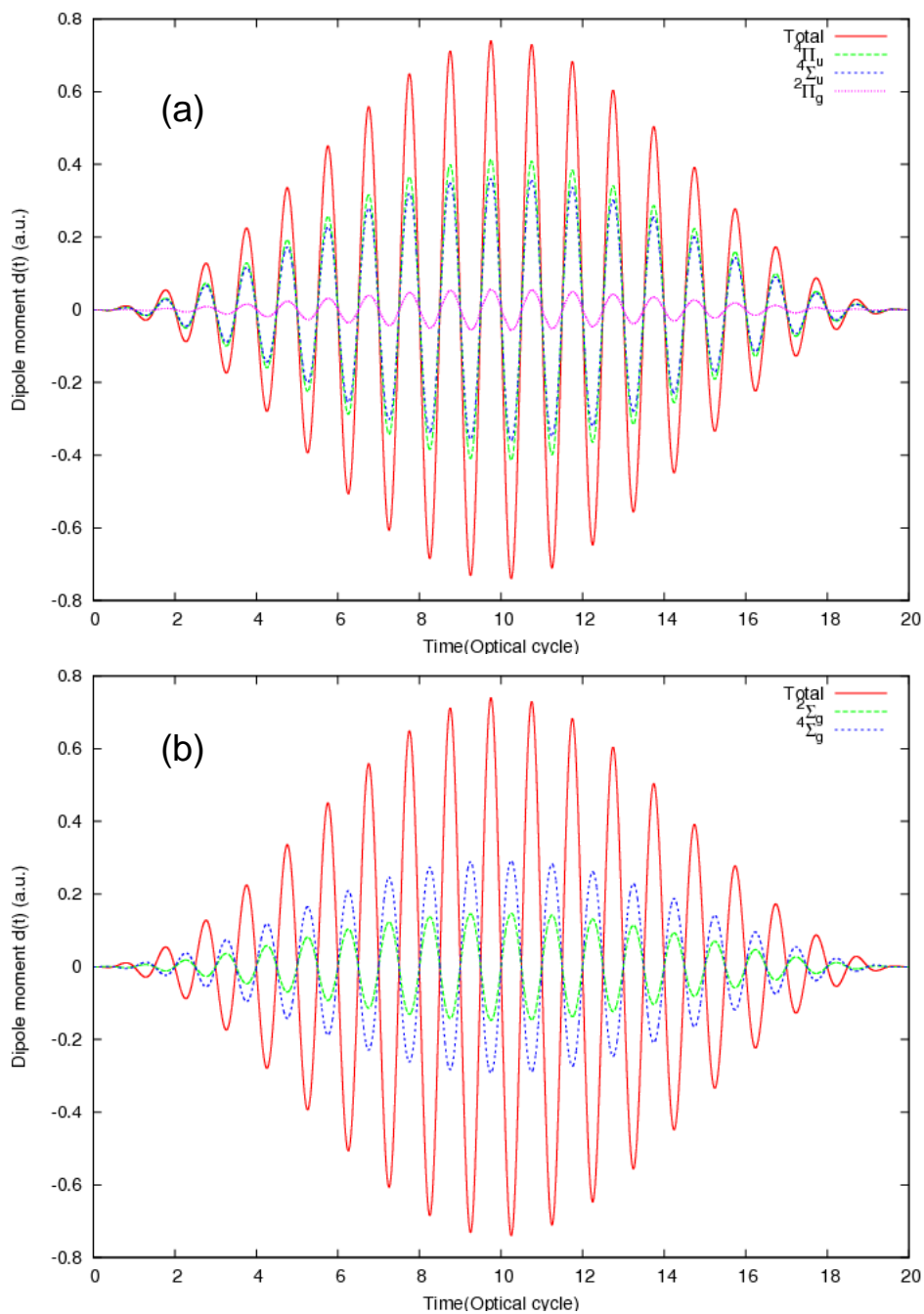


Figure 4-9 Comparison of the induced dipole moment of  $O_2$  from different spin orbital in  $10^{14} \text{ W/cm}^2$ ,  $800\text{nm}$ ,  $\sin^2$  laser pulses

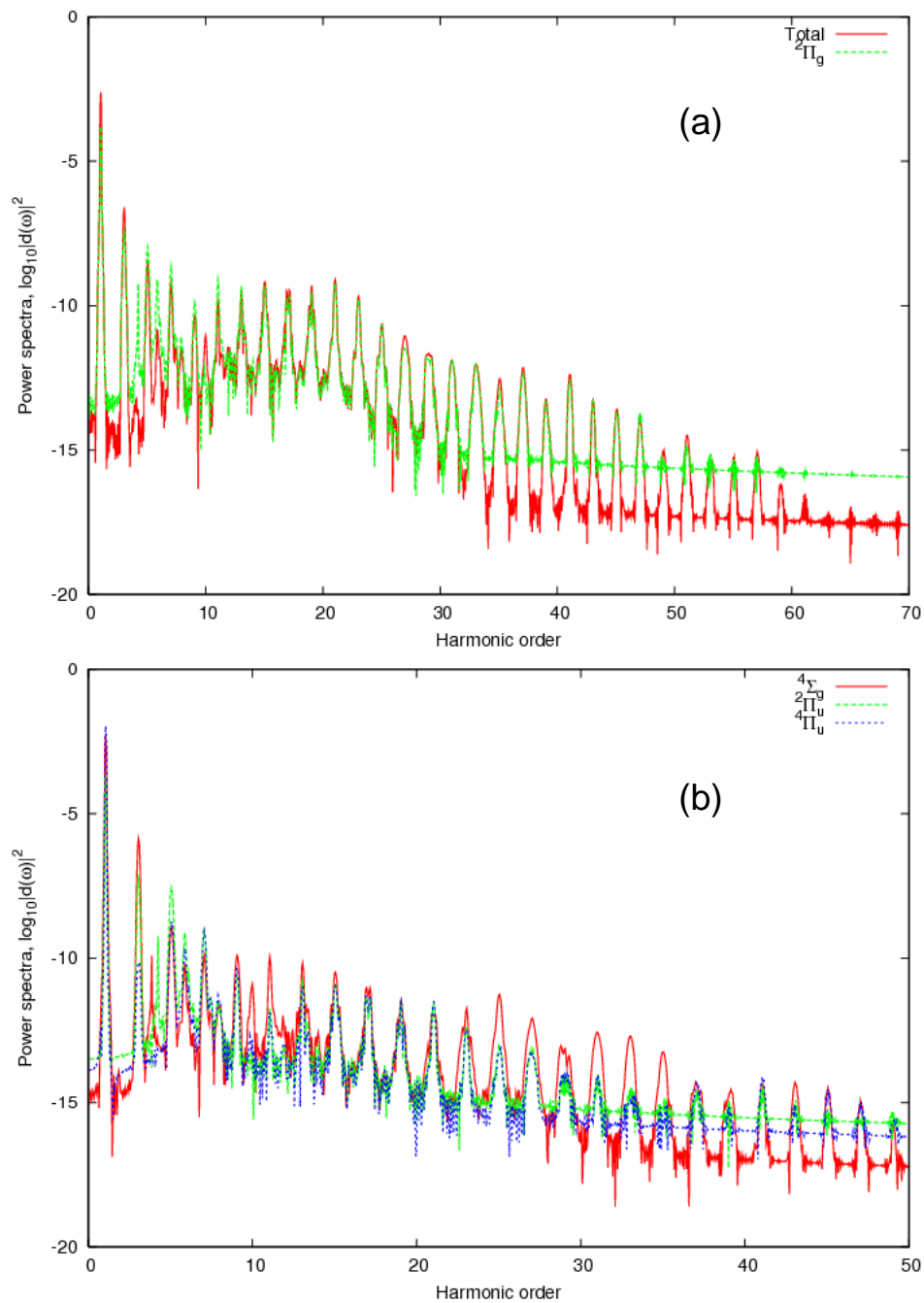


Figure 4-10 (a) Comparison of the total HHG power spectrum and the partial contributions from HOMO of  $O_2$ , and (b) from different spin orbital in  $10^{14} \text{ W/cm}^2$ , 800nm,  $\sin^2$  laser pulses

To investigate the detailed spectral and temporal structure of HHG, we perform the time-frequency analysis by the wavelet transform of the total induced dipole moment  $d(t)$ ,

$$A_w(t_0, t) = \int d(t)W_{t_0, \omega}(t)dt \equiv d_w(t), \quad (4.6)$$

$$W(x) = (1/\sqrt{\tau})e^{ix}e^{-x^2/2\tau^2}, \quad (4.7)$$

The parameter  $\tau= 15$  is chosen to perform the wavelet transformation in the following study. In Figure 4-11, the time profiles show series of peaks separated by about half the laser period. These peaks, which indicate the instants (during the laser excitation) at which the harmonic is emitted. For both  $N_2$  and CO molecules, the emissions take place near the center of the laser field envelope. For the  $N_2$  molecule, it shows that every half-cycle high-order harmonics are emitted, and the harmonics are partially synchronized as their peaks appears at slightly different time position. For the CO molecules, the number of dominant emissions per optical cycle is now limited to only one. This result is in contrast with the strong field recollision model [44] which state that every half-cycle the electron wave packet returns for a recollision with the molecular core. The CO molecule also appear to have more synchronized harmonics

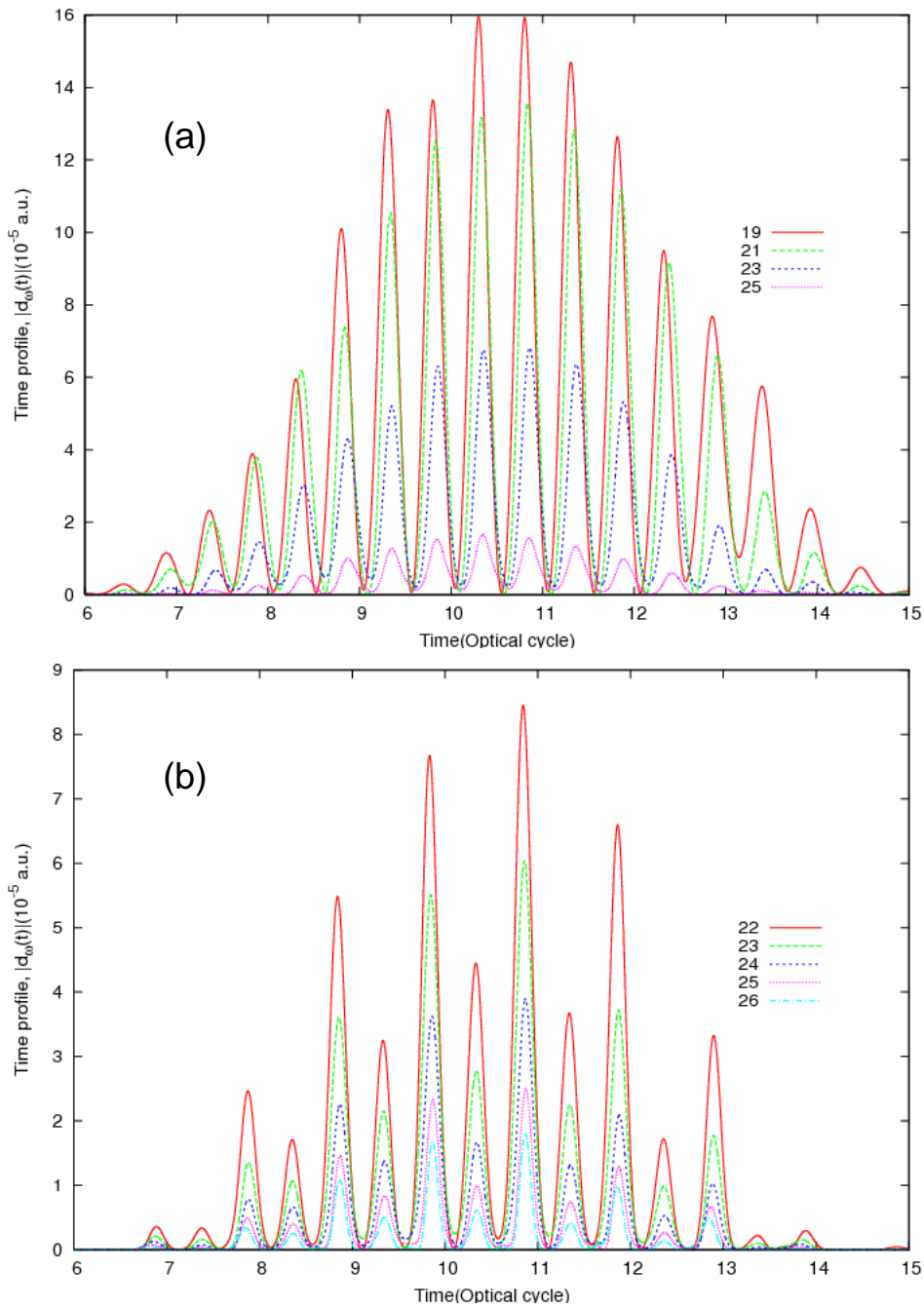


Figure 4-11 Time profiles for (a)  $N_2$  and (b) CO. Laser intensity used is  $10^{14} \text{ W/cm}^2$ , wavelength used is 800nm, with 20-optical-cycle in pulse duration.



## 4.4 OCT on two-level system

A two-level system consists of two orthonormal states  $|a\rangle$  and  $|b\rangle$ . The state vector at time  $t$  is given by

$$|\Psi(t)\rangle = c_a(t)|a\rangle + c_b(t)|b\rangle = \begin{pmatrix} c_a(t) \\ c_b(t) \end{pmatrix} \quad (4.8)$$

The time evolution of  $|\Psi(t)\rangle$  is described by the time-dependent Schrödinger equation with the Hamiltonian in the basis  $|a\rangle$  and  $|b\rangle$  given by

$$\hat{H}(t) = \begin{pmatrix} \omega_a & 0 \\ 0 & \omega_b \end{pmatrix} - \varepsilon(t) \begin{pmatrix} 0 & \mu \\ \mu & 0 \end{pmatrix}, \quad (4.9)$$

For an arbitrary laser field  $\varepsilon(t)$ , the time-dependent wavefunction is only numerically solvable.

We start with the final-time control. The initial wavefunction is in state  $|a\rangle$ . We want it to end in state  $|b\rangle$  after the interaction with the electric field. Thus the target operators are  $\hat{O}_1 = |b\rangle\langle b|$  and  $\hat{O}_2 = 0$ . Standard scheme is used here.

Figure 4-12(b) shows the population is completely transferred from state  $|a\rangle$  to  $|b\rangle$  and the optimized laser field in Figure 4-12(a) is monochromatic as expected.

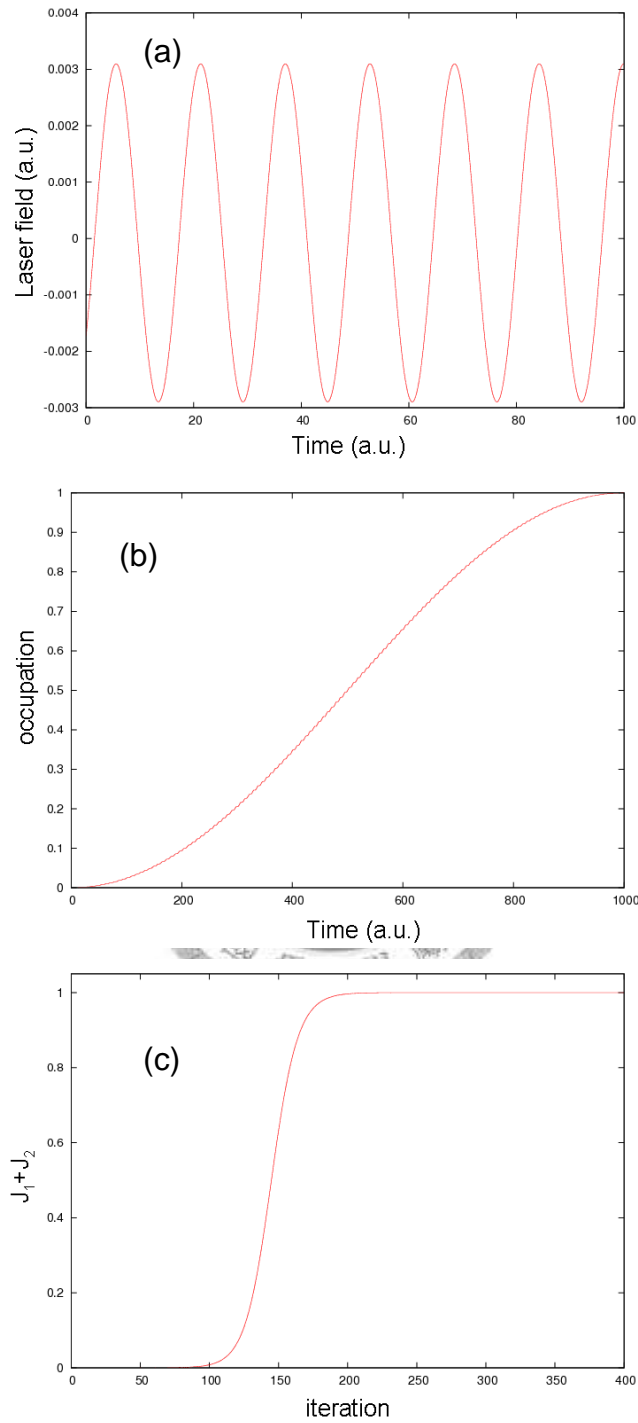


Figure 4-12 Optimization of the  $|a\rangle \rightarrow |b\rangle$  transition. (a) Optimized field. (b) Time evolution of the occupation numbers for the system propagated with the optimized pulse. (c) Convergence of  $J_1$  and  $J_2$  over the iterations.

The time-dependent target wave function is chosen as

$$|\phi(t)\rangle = \alpha(t)e^{-i\varepsilon_0 t}|a\rangle + \beta(t)e^{-i\varepsilon_0 t}|b\rangle \quad (4.10)$$

,

where the coefficients  $\alpha(t)$  and  $\beta(t)$  are real and satisfy the following relations

$\alpha^2(t) + \beta^2(t) = 1$ ,  $\hat{O}_1 = 0$ ,  $\hat{O}_2 = |\phi(t)\rangle\langle\phi(t)|$ . We apply the conjugate gradient method to this scheme.

From Figure 4-12 to 4-14, we can see the controlling results of different type targets are all quite successful. The first result in Figure 4-12 using standard scheme with the rather simple final-time target takes about 400 iterations to reach the numerical convergence. While the other two time-dependent targets combined with conjugate gradient method, the iterations needed are greatly reduced to less than a hundred.



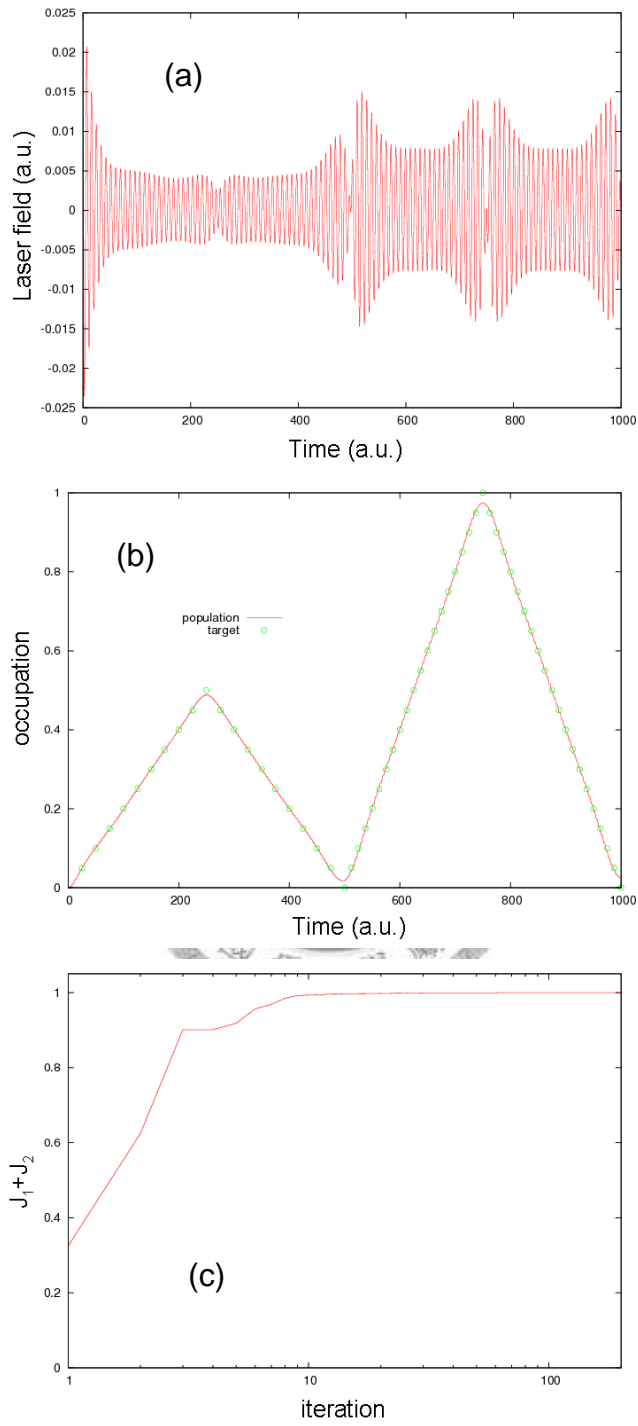


Figure 4-13(a) Optimized field. (b) Targets and time evolution of the occupation numbers. (c)

Convergence of  $J_1$  and  $J_2$  over the iterations

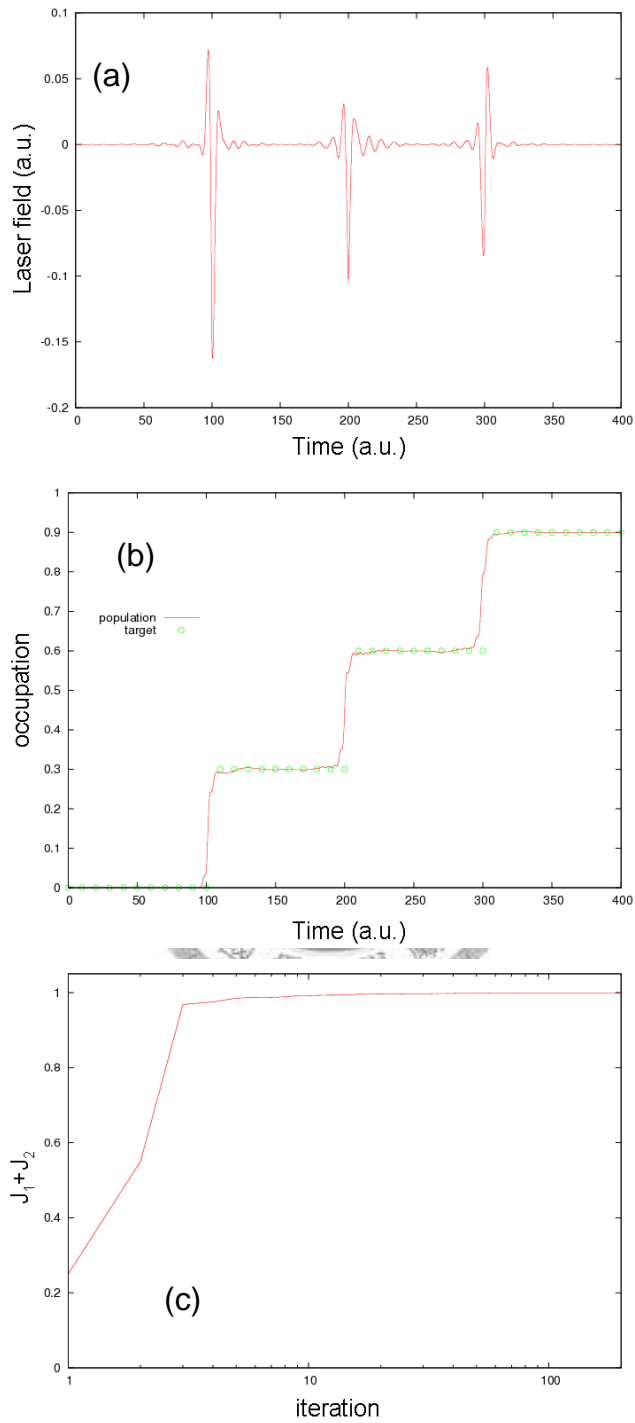


Figure 4-14(a) Optimized field. (b) Targets and time evolution of the occupation numbers. (c)

Convergence of  $J_1$  and  $J_2$  over the iterations

# Chapter 5

## Conclusion and perspectives

We use the generalized pseudospectral method to treat TDDFT equations accurately and efficiently. Calculations on MPI and HHG of diatomic molecules are presented. The ionization potential of each orbital has been accurately treated with correct asymptotic long-range effective potential using  $LB\alpha$  exchange-correlation potential. We have observed that ionization potential is not the only dominate factor of the ionization rate in diatomic molecules. In certain laser intensities, the orientation of the molecular orbitals changes the order of ionization. The detailed HHG spectrum and time profiles are analyzed by the wavelet transformation. The major contributions to the higher order harmonics are from HOMO which is ionized most. We also see the first order Stark effect from the permanent dipole moment of the CO molecule causes the large ionization probability. Moreover, breaking of the inversion symmetry produces even-order harmonics and allows only one main emission in one optical cycle.

HHG is related to the generation of many modern laser techniques. Our final goal is to control and enhance the intensity of a specific harmonic. In this thesis, we have presented realistic two-energy level of systems that of atoms or diatomic molecules and have successfully manipulate the optimal control theory. Both final-time and time-dependent control have match the targets more than 99%. Introduction of the conjugate gradient method into the OCT greatly reduces the iterations needed to reach convergence.

# Bibliography

- [1] T. Brabec, and F. Krausz, *Reviews of Modern Physics* **72**, 545 (2000).
- [2] C. Spielmann *et al.*, *Science* **278**, 661 (1997).
- [3] I. P. Christov, M. M. Murnane, and H. C. Kapteyn, *Physical Review Letters* **78**, 1251 (1997).
- [4] C. Gohle *et al.*, *Nature* **436**, 234 (2005).
- [5] S. T. Cundiff, and J. Ye, *Reviews of Modern Physics* **75**, 325 (2003).
- [6] D. PaviCic *et al.*, *Physical Review Letters* **98**, 243001 (2007).
- [7] X. M. Tong, Z. X. Zhao, and C. D. Lin, *Physical Review A* **66**, 033402 (2002).
- [8] H. R. Reiss, *Physical Review A* **22**, 1786 (1980).
- [9] J. Muth-Bohm, A. Becker, and F. H. M. Faisal, *Physical Review Letters* **85**, 2280 (2000).
- [10] K. J. Schafer, and K. C. Kulander, *Physical Review A* **42**, 5794 (1990).
- [11] M. J. DeWitt, E. Wells, and R. R. Jones, *Physical Review Letters* **87**, 153001 (2001).
- [12] E. Wells, M. J. DeWitt, and R. R. Jones, *Physical Review A* **66**, 013409 (2002).
- [13] C. A. Ullrich, U. J. Gossmann, and E. K. U. Gross, *Physical Review Letters* **74**, 872 (1995).

- [14] X.-M. Tong, and S.-I. Chu, Physical Review A **57**, 452 (1998).
- [15] X.-M. Tong, and S.-I. Chu, Physical Review A **64**, 013417 (2001).
- [16] R. S. Judson, and H. Rabitz, Physical Review Letters **68**, 1500 (1992).
- [17] C. J. Bardeen *et al.*, Chemical Physics Letters **280**, 151 (1997).
- [18] S. Vajda *et al.*, Chemical Physics **267**, 231 (2001).
- [19] R. Bartels *et al.*, Nature **406**, 164 (2000).
- [20] J. L. Herek *et al.*, Nature **417**, 533 (2002).
- [21] G. M. Huang, T. J. Tarn, and J. W. Clark, Journal of Mathematical Physics **24**, 2608 (1983).
- [22] A. P. Peirce, M. A. Dahleh, and H. Rabitz, Physical Review A **37**, 4950 (1988).
- [23] P. Hohenberg, and W. Kohn, Physical Review **136**, B864 (1964).
- [24] W. Kohn, and L. J. Sham, Physical Review **140**, A1133 (1965).
- [25] J. P. Perdew, and Y. Wang, Physical Review B **45**, 13244 (1992).
- [26] X. Chu, and S.-I. Chu, Physical Review A **63**, 023411 (2001).
- [27] X. Chu, and S.-I. Chu, Physical Review A **70**, 061402 (2004).
- [28] John Heslar *et al.*, International Journal of Quantum Chemistry **107**, 3159 (2007).
- [29] D. A. Telnov, and S.-I. Chu, Physical Review A (Atomic, Molecular, and Optical Physics) **76**, 043412 (2007).
- [30] X. Chu, and S.-I. Chu, Physical Review A **64**, 063404 (2001).



- [31] edited by M. Abramowitz and I. Stegun (Dover, New York, 1965).
- [32] D. A. Telnov, and S.-I. Chu, *Physical Review A* **71**, 013408 (2005).
- [33] X.-M. Tong, and S.-I. Chu, *Chemical Physics* **217**, 119 (1997).
- [34] X. Chu, and S.-I. Chu, *Physical Review A* **63**, 013414 (2000).
- [35] V. Ramakrishna *et al.*, *Physical Review A* **51**, 960 (1995).
- [36] W. Zhu, J. Botina, and H. Rabitz, *The Journal of Chemical Physics* **108**, 1953 (1998).
- [37] W. Zhu, and H. Rabitz, *The Journal of Chemical Physics* **109**, 385 (1998).
- [38] Y. Ohtsuki, G. Turinici, and H. Rabitz, *The Journal of Chemical Physics* **120**, 5509 (2004).
- [39] I. Serban, J. Werschnik, and E. K. U. Gross, *Physical Review A* **71**, 053810 (2005).
- [40] R. Kosloff *et al.*, *Chemical Physics* **139**, 201 (1989).
- [41] A. Lofthus, and P. H. Krupenie, *Journal of Physical and Chemical Reference Data* **6**, 113 (1977).
- [42] P. Baltzer *et al.*, *Physical Review A* **45**, 4374 (1992).
- [43] A. B. Cornford *et al.*, *The Journal of Chemical Physics* **54**, 2651 (1971).
- [44] X.-M. Tong, and S.-I. Chu, *Physical Review A* **61**, 021802 (2000).

